Abstract

Silicone oil droplets containing synthetic smectite clay submerged in another immiscible organic oil have been studied by observing clay particle movement, oil circulation and drop deformation when an electric field is applied. Results show how electric field strength, electrohydrodynamics, dielectric and conductive properties determines the fluid flow, clay particle formation and drop deformation.

Acknowledgements

I firstly wish to thank professor Jon Otto Fossum for good guidence and his enthusiasm, and also for making it possible to collaborate with other physicists in the same area of research, both nationally and internationally.

Thanks to Paul Dommersnes at Universite Paris 7 who have helped explain and suggested relevant theory, in addition to experimental advice. Thanks to Rene Castberg at UiO for helping out with programming scripts in MATLAB and sharing results of his research. Lastly thanks to Zbigniew Rozynek at NTNU for sharing work results, giving helpful advice and inspiration.

Contents

Chapter 1

Introduction

Electric fields can induce fluid motion, and conversely, fluid flow can result in an electric field[1]. A wide range of applications makes use of this interaction between fluids and electric fields, e.g. electrosprays, ink-jet printing and electrohydrodynamic(EHD) pumps. EHD systems often rely on the interaction between the electric field and fluid drops[2]. Liquid drops have several responses when affected by an electric field, like deformation, rotation, coalescence or breakup, which are not yet fully understood. These reactions are important when it comes to emulsions and electrorehological(ER) fluids. By controlling the drop-fluid reactions, one can help stabilize or destabilize emulsions. Stable emulsions are important in several areas, e.g. preparation of foods and cosmetics, to the manufacturing of plastics, while destabilzing emulsions have practical uses in the oil industry by dehydrating crude oil or in digital microfluids, where drops are used as carriers[3]. ER fluids also have several uses, for example being used in hydrolic valves and brakes or in shock absorbers[4, 5, 6].

The study of clay is the main theme in our research group, and our main motivation is that clays may be viewed as good representative model systems for soft condensed matter and complex materials, with 'near' applications. The purpose of this project is to see how adding smectite clay particles to a drop will affect its response in an electric field.

Chapter 2

Theory of liquid circulation, movement and drop deformation induced by electric fields

To better understand the effects of eletric fields on electrorheological(ER) drops, we start by looking at some theory concerning the effects of electric fields on pure drops, i.e. no smectite clay added in the oil drops. O'Konski and Tacher where the first to develop a model for droplet deformation in an eletric field, called the perfect dielctric model(1953)[7], which describes prolate(longer in the direction of the electric field) droplets. During their experiments they also encountered oblate droplets, i.e. opposite of prolate droplets. This was later described by Taylor(1966)[8] which developed a model which is now known as the leaky dielectric model. If the deformation is high enough, drop break-up can occur. For sufficiently high fields another phenomenon is observed, the droplet can start spinning spontanously, which resembles what Quincke observed for solid dielectrics in 1896[9].

2.1 Dielectric sphere in electric field

A natural start for understanding electric field effects on droplets, is to look at a static solid dielectric sphere inside a dielectric medium, when a uniform electric field is applied. We can derive a solution for this electrostatic example by expressing the electric field $\vec{E}$ as a electric potential V and by applying Maxwell's equations as shown in [10]. The potential is related to the field as

$$\vec{E} = -\nabla V. \tag{2.1}$$

We have Gauss' law as:

$$\nabla \cdot \vec{E} = \frac{\rho}{\epsilon_0} \tag{2.2}$$

where ρ is the charge density and ϵ_0 is the vacuum permitivity. With no free charges, operating with ∇ and combining eq. (2.2) with eq. (2.1) we get:

$$\nabla^2 V = 0 \tag{2.3}$$

The boundary conditions for the dielectric sphere with radius a in the dielectric medium is:

$$V_{in} = V_{out}, \qquad \text{for r=}a \tag{2.4}$$

$$\epsilon_{in} \frac{\partial V_{in}}{\partial r} = \epsilon_{out} \frac{\partial V_{out}}{\partial r}, \qquad \text{for r=}a \tag{2.5}$$

$$V_{out} \to -E_0 r \cos\theta, \qquad \text{for r} \gg a \tag{2.6}$$

where E_0 is the applied field far away, and r and θ is the distance from the center of the sphere and angle from the field direction through the center of the sphere respectively. ϵ_{in} is the permittivity inside the sphere, and ϵ_{out} is the permittivity in the surrounding medium. The derivation of eq. (2.3) with the given boundary conditions can be found in Appendix A.1. From this we can see the potential inside the sphere is

$$V_{in}(r,\theta) = -\frac{3\epsilon_{out}E_0}{\epsilon_{in}+2\epsilon_{out}} r\cos\theta = -\frac{3\epsilon_{out}E_0}{\epsilon_{in}+2\epsilon_{out}} z, \tag{2.7}$$

which means we have a uniform field inside the sphere:

$$\vec{E} = \frac{3\epsilon_{out}}{\epsilon_{in}+2\epsilon_{out}} \vec{E_0}. \tag{2.8}$$

The potential from the induced dipole outside the sphere is

$$V = \frac{B_1 \cos\theta}{r^2}, \tag{2.9}$$

while the potential of a general dipole field is

$$V = \frac{p \cos\theta}{4\pi\epsilon_0 r^2}. \tag{2.10}$$

Combining eqs. (2.9) and (2.10) we then get the total dipole moment

$$\vec{p} = 4\pi\epsilon_0 \frac{\epsilon_{in} - \epsilon_{out}}{\epsilon_{in} + 2\epsilon_{out}} a^3 \vec{E_0} \tag{2.11}$$

where we used the expression for B_1 from eq. (A.18).

The total dipole is equal to the volume integral of the the polarization $\vec{P}$ inside the sphere. The electric field and the polarization is constant inside the sphere, and can be found:

$$\vec{P} = \frac{p}{\frac{4}{3}\pi a^3} = 3\epsilon_0 \frac{\epsilon_{in} - \epsilon_{out}}{\epsilon_{in} + 2\epsilon_{out}} \vec{E_0} \tag{2.12}$$

As we can see $\vec{P}$ is parallel to $\vec{E_0}$, the polarization charge on the surface of the sphere is then

$$q_\sigma = \vec{P} \cdot \hat{n} = P \cos\theta. \tag{2.13}$$

From eq. (2.13) we see that we get positive surface charges on one side(pole), and negative charges on the other side(pole), so that the sphere has been made into a dipole. The electric field lines inside and outside can be seen in figure 2.1.

2.2 The perfect dielectric model

O'Konski and Thacher developed a model for droplet deformation in an electric field in a study in 1953[7]. They observed a prolate deformation of drops submerged in a dielectric fluid when an electric field was applied. They described the deformations as a result of the surface energy and the electric potential energy of the ellipsoid. Allan and Mason(1962)[11] did also develop a model for the deformation of droplets, by balancing electrical and interfacial tension

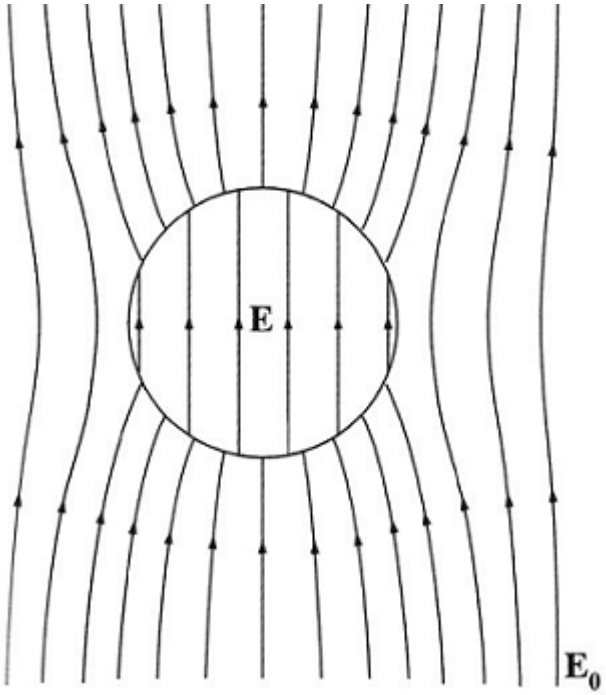

Figure 2.1: Shows electric field lines in and around sphere when a homogenous electric field is applied. Figure taken from [10].

forces. Both methods give the same model for small deformations in *conducting* drops in a dielectric medium:

$$D = \frac{9}{16}\frac{a\epsilon_{out}\epsilon_0 E_0^2}{\gamma} \tag{2.14}$$

where ϵ_{out} is the surrounding fluids relative permittivity, ϵ_0 the vacuum permittivity, E_∞ is the applied field strength, a is the droplet radius, γ is the interfacial tension and D of course is the deformation. The deformation is defined as the difference in lengths of the droplet parallel and transverse to the applied field, divided by the sum of the two lengths, or just:

$$D = \frac{d_\parallel - d_\perp}{d_\parallel + d_\perp} \tag{2.15}$$

Where $d_\parallel$ is the length across the droplet parallel to the electric field, and $d_\perp$ is the length transverse to the field. $D > 0$ gives a prolate shape, and $D < 0$ gives and oblate shape. For the conducting droplet the pressure inside and outside is uniform, and is initially balanced by the interfacial tension and the sphere's curvature, $2\gamma/a$. The non-uniform electric stresses must therfore be balanced by interfacial tension on the droplet surface. The sphere induces a dipole which varies as $\cos\theta$, θ is the angle from the direction of the applied electric field, and thus a field normal to the surface creates a stress that varies as $\cos^2\theta$, which will stretch the droplet along the direction of the applied field, giving it a prolate deformation. For *dielectric* droplets in dielectric mediums, Allan and Mason found the deformation to be

$$D = \frac{9}{16}\frac{a\epsilon_{out}\epsilon_0 E_0^2}{\gamma}\frac{(\epsilon_{in}-\epsilon_{out})^2}{(\epsilon_{in}+2\epsilon_{out})^2}. \tag{2.16}$$

In this case, the induced dipole charges on the droplet surface varies as we found in eq. (2.13). The field will then pull the charges at each pole in opposite directions, and give the droplet a prolate deformation. In both cases, the deformation depends on E^2, so a reversal of the field will give the same deformation. However, Allan and Mason also witnessed oblate deformations when it came to the dielectric droplets, and the perfect dielectric model couldn't predict this. This led Taylor(1966) to believe that the surrounding carrying fluid couldn't be viewed as an insulator, and led to his development of the leaky dielectric model which we will discuss next.

2.3 Taylor's leaky dielectric model

It doesn't seem possible for a drop to exist at rest in equilibrium in an electric field, neither the surface tension nor constant internal and external pressures can balance the stress due to the electric field, which varies over the surface of the drop[8]. So for the drop to keep its spherical shape, the electric stress must be balanced by variable pressure difference between the inside and the outside of the drop. For such a pressure difference to exist, the fluids inside and outside the drop must be in motion.

Taylor assumed that the potential in and around the droplet could be approximated by the potential in and around that of a static *conducting* sphere submerged in a conducting fluid. This assumtion can be made since the fluid motion which convect charge is relative slow compared to the electic charge conduction, and in most cases the effects of charge convection is likely to be small.

The potential for this case is given as[8]

$$V_{in} = \frac{3}{2+R} E_0 r \cos\theta$$

$$V_{out} = \left(r + \frac{1-R}{2+R} \frac{a^3}{r^2} \right) E_0 \cos\theta$$

where R is the ratio of conductivity between the two fluids, $R \equiv \sigma_{in}/\sigma_{out}$. As we can see the potentials are quite similar to the potentials of a dieletric, eqs. (A.19) and (A.20). The fluids are assumed to exhibit normal ohmic resistance, and the electric field will therefore look the same as for the dielectric case, figure 2.1. Build up of surface charges happens in the following manner. Firstly, assume no electric field, then both fluids, drop and surrounding fluid, will be electrically neutral. If the droplet has higher conductivity than the outer fluid, charges inside the droplet will reach the interface between the droplet and surrounding fluid faster than the charges in the surrounding fluid, the free charges that build up at the interface cause a reduced field inside the drop, for the opposite case, when the conductivity is lower inside the droplet than outside, the field inside the droplet is enhanced. After a while, when the current on both sides of the interface is equal, the system is stationary.

The surface charges cause the electric field to exert a stress on the interface, so this is where the fluid motion comes in. The stress caused by the electric field acts both normally and tangentially at the interface, since surface tension only acts normally, Taylor suggested that the tangential electric stress must be balanced by hydrodanamic currents inside and outside the drop.

The normal component of the electric field at the droplet interface is what causes prolate or oblate shape. The tangential component of the electric field has to be continous across the interface boundary. The tangential field at the interface is a projection of the field inside the droplet, and this was found to be uniform, eq. (2.8). At the poles($\theta = 0, \pi$), the tangential field is therefore zero, since here the interface surface is orthogonal to the field inside the droplet. The tangential field increases towards and at max at the equator($\theta = \pi/2$), where the interface surface is parallel to the field inside the droplet. Even though the tangential component of the field is strongest at the equator, there is no tangential stress here, this is due to the fact that all the charges are drawn against the poles, and at the equator no charges have built up. The tangential stress is then balanced by viscous flow in the same direction as the electric stress. This results in a flow along the interface from pole to the equator, or

the other way around. Viscosity balances the flow by creating a drag in the opposite direction. The deformation(eq. (2.15)) Taylor found to be

$$D = \frac{9}{16}\frac{a\epsilon_{out}\epsilon_0 E_0^2}{\gamma S(2+R)^2} \times \left[S(R^2+1) - 2 + 3(RS-1)\left(\frac{3M+2}{5M+5}\right)\right], \tag{2.19}$$

where $S \equiv \epsilon_{out}/\epsilon_{in}$ is the permittivity ratio and $M \equiv \eta_{out}/\eta_{in}$ is the viscosity ratio, R still is σ_{in}/σ_{out}. Since all terms are positive, we can see that the term in the brackets, and only R, S and M, decides if the deformation is oblate or prolate:

$$\phi(S,R,M) = S(R^2+1) - 2 + 3(RS-1)\left(\frac{3M+2}{5M+5}\right). \tag{2.20}$$

Prolate deformations happen when $\phi > 0$, and oblate when $\phi < 0$. Rewriting (2.19) gives

$$D = \frac{9}{16}\frac{a\epsilon_{out}\epsilon_0 E_0^2}{\gamma S(2+R)^2}\phi, \tag{2.21}$$

where ϕ is (2.20). The tangential velocity on the drop surface was according to Taylor,

$$\upsilon_\theta = -\frac{9}{8\pi}\frac{a\epsilon_{in}E_0^2}{(2+R)^2}\frac{RS-1}{5(\eta_{in}+\eta_{out})}sin(2\theta). \tag{2.22}$$

The direction of the flow is from the equator to the poles when υ_θ is positive, i.e. when $RS < 1$. From the equation we can see that the velocity is zero at the equator and at the poles. The maximum velocity is found at $\theta = 45°$. An illustration of the viscous viscous flow, and its direction for a case when $RS < 1$ and the charge relaxation time($\tau = \epsilon/\sigma$) is higher in the droplet than in the supporting fluid, can be seen in figure 2.2. We will discuss charge relaxation time and its effects more in section 2.6.

In alternating fields the deformation consists of a steady and an oscillatory part, where the steady deformation has been given by Torza *et al.* to be the same as eq. (2.21)[12], except ϕ is given as

$$\phi = 1 - \frac{S^2R(11+14M) + 15S^2(1+M) + S(19+16M) + 15R^2S\tau^2\omega^2(M+1)(S+2)}{5(M+1)[S^2(2+R)^2 + R^2\tau^2\omega^2(1+S)^2]} \tag{2.23}$$

where ω is the frequency and τ is a hybrid relaxation time equal to $\frac{\epsilon_{out}}{\sigma_{in}}$. According to eq. (2.23) the steady deformation can vanish at a certain frequency, and shift between prolate and oblate deformation depending on the frequency. If the frequency is alot higher than the Maxwell time($\frac{1}{\tau}$), it is clear that there will

be no charge buildup at the drop-fluid interface like the one happening in the leaky dielectric case, and the deformation will be just as in a perfect dielectric case.

To summarize, in a perfect conducting or a perfect dielectric sphere, the electric stress will always be normal to the surface, while for a leaky dielectric the electric stress will have a tangential component in addition to the normal component. The addition of this tangential component, results in tangential flow.

The circular flow patterns in Taylors' leaky dielectric model has been supported by a photographs done by McEwan and de Jong, which was presented in an addendum to Taylor's paper[8]. Comparing Taylor's model with the results found by Allan and Mason(1962) gave a qualitative agreement between Taylor's theory and Allan and Mason's observations in nine of the thirteen cases studied. A later study by Torza et al.(1971)[12], also showed qualitative agreement with experiments, but the quantitative aspects of the theory were not in good agreement with the results. The deformation varied linearly with aE_∞^2 as predicted, but the proportionality factor exceeded the theoretical value in almost all cases. The slopes were also larger than the theoretical value, one case as much as four times the theoretical value.

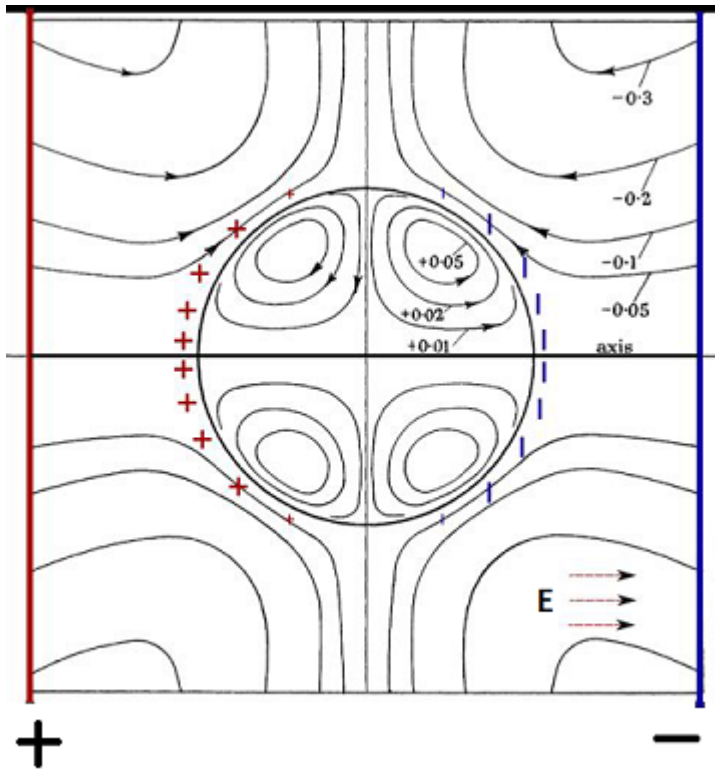

Figure 2.2: Taylor's Leaky Dielectric Model - Shows viscous flow and direction when $RS < 1$. The density of fieldlines indicates flow velocities. Figure adapted from [8].

2.4 Drop break-up

For high enough fields, the deformation can be so large that the drop breaks up. Allan and Mason observed three types of deformation and break-up patterns depending on the dielectric and conductive properties[11]. The three observed types of deformation were: (1) For conductive drops in a dielctric oil the drop deformed symmetrically, and eventually seperated into two almost equal parts. (2) For dielectric drops and surrounding fluid with $RS > 1$, the deformation was asymmetrical, with one side of the drop remaining spherical, whilst the other was stretch out like a thread. This liquid thread streched out towards the negative electrode and small drops broke off. The stretching towards the negative electrode indicates negative charge leakage from the other side of the drop. (3) For dielectric drops and surrounding fluid with $RS < 1$, the drop flattened(oblate) and eventually folded and broke up into uneven parts. An illustration of the three different types of break-up can be seen in figure 2.3.

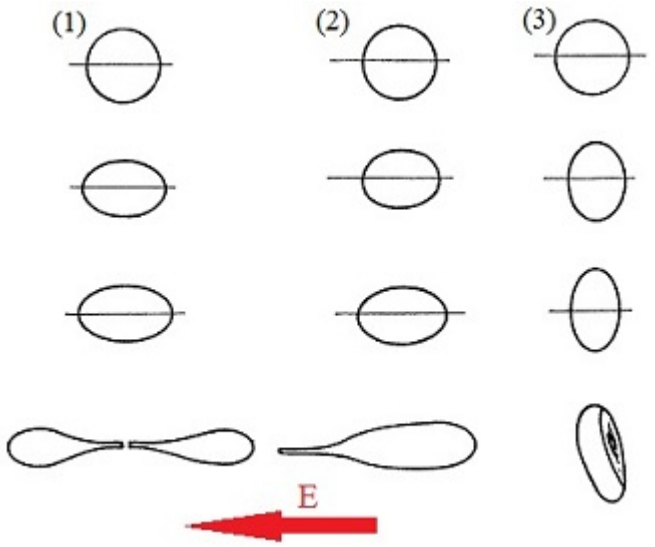

Figure 2.3: Illustrates the three types of break-up. (1) Conductive drop in dielectric oil. (2) Dielectric drop and surrounding fluid with $RS > 1$. (3) Dielectric drop and surrounding fluid with $RS < 1$. Figure adapted from [11]

.

2.5 Formation of clay ring around drop

A previous project report on this subject written by myself showed for the clay-oil drop case that the viscous flow occuring when applying a low DC electric field(<250 V/mm), resulted in the clay particles following flow lines similar to the ones described in the leaky dielectric model, and gradually gathering at the drop surface around the equator forming a ring/ribbon. An example of this ring can be seen in figure 2.4. An illustration showing the flowlines around the drop, indicating that it is flow similar to leaky dielectric flow, can be seen in figure 2.5.

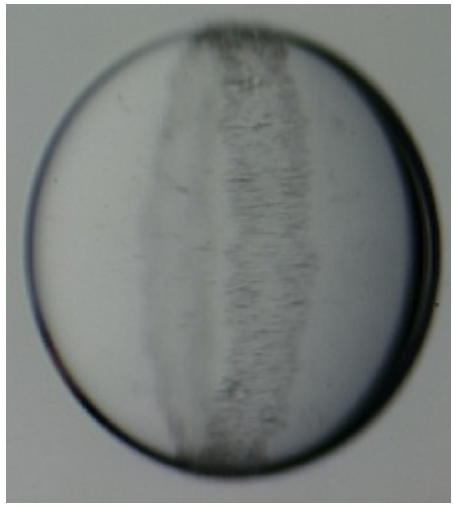

Figure 2.4: Ribbon formation seen from a ∼30 degree angle from the perpendicular view to the electric field.

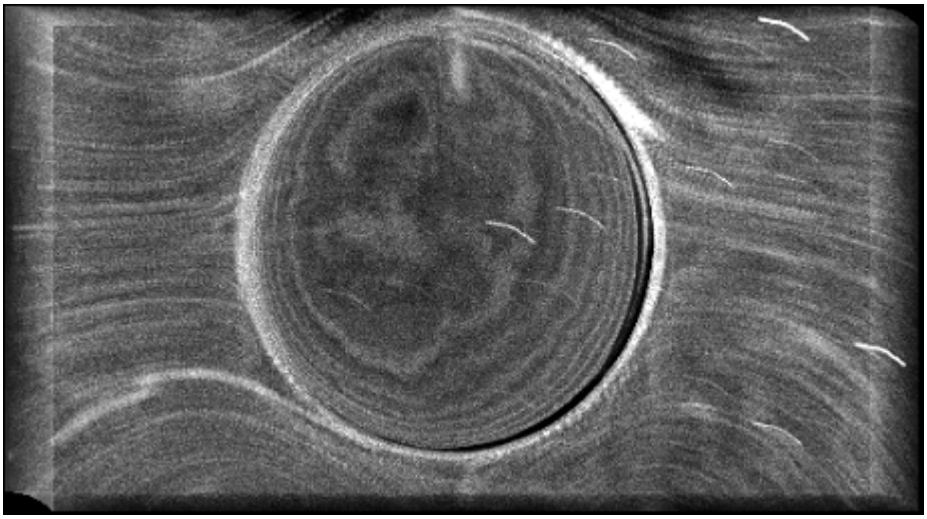

Figure 2.5: Illustration of flow around drop. Image made from several frames from the same video, so that particles appear as flowlines. Flowlines resembles those described in the leaky dielectric model.

2.6 Drop rotation

Taylor's leaky dielectric model has proven to be quite useful for small fields, but for stronger fields a nonaxisymmetric rotational flow can be seen, which isn't described by Taylors model. This phenomena resembles that of the rotation of a solid dielectric particle observed by Quincke(1896)[9].

From Taylors model, we remember that the value of RS determined the direction of the flow. If we rewrite RS to charecterize the conduction response of the fluids, we get

$$RS = \frac{\tau_{out}}{\tau_{in}} \tag{2.24}$$

where $\tau_{out} = \frac{\epsilon_{out}}{\sigma_{out}}$ and $\tau_{in} = \frac{\epsilon_{in}}{\sigma_{in}}$ is the charge relaxation time outside and inside the droplet respectively. As before, if $RS > 1$, $(\tau_{in} < \tau_{out})$, the conduction in the drop is better than in the surrounding fluid, and the charge distribution at the interface will be dominated by charges from inside the droplet, and as this will cause the dipole moment to align with the external electric field, causing the surface charges to be drawn towards the electrodes creating the external field, and the again causing the droplet poles to be stretched outwards and only prolate deformation can occur. For the other case, $RS < 1$, the opposite happens, and the charge distribution at the interface is dominated by charges from the surrounding fluid, causing the dipole to be reversed, and thus causing the surface charges to be drawn towards the equator. For this case both prolate and oblate deformation can occur. An illustration of this can be seen in figure 2.6.

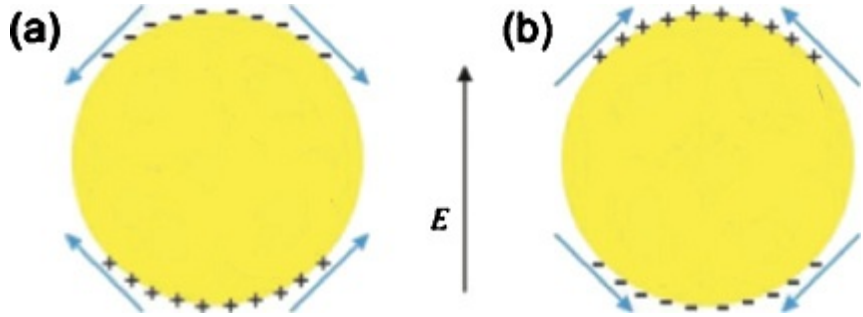

Figure 2.6: Illustration of surface charge distribution and the direction of fluid motion at the surface for (a)$RS < 1$ and (b) $RS > 1$. Figure taken from [2].

For $RS < 1$, the reversed dipole causes an unstable state. The dipole will

above some critical field be displaced and this will cause a torque which again will cause the drop to rotate. The surface charges will rotate with the drop, and at the same time charges will be applied to the droplet interface by the suspending fluid. The balance between the charge convection caused by fluid motion and the charges applied from the suspending fluid gives rise to a dipole orientation which is no longer parallel to the electric field and cause a continous rotational motion. In figure 2.7 we can see an illustration of the quincke effect.

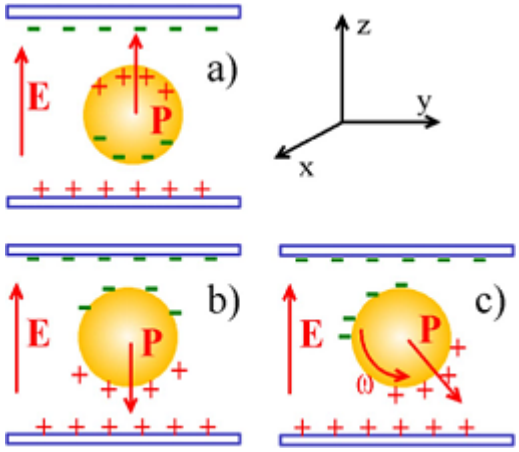

Figure 2.7: Dipole orientation due to interfacial charge distribution: (a) The charge relaxation time is smaller in the particle than in the host liquid($\tau_{in} < \tau_{out}$), $\vec{P}$ is parallel to $\vec{E}$. (b) the charge relaxation time is higher in the particle than in the host liquid($\tau_{in} > \tau_{out}$), $\vec{P}$ is antiparallel to $\vec{E}$. (c) when $\vec{P}$ is antiparallel to $\vec{E}$, the equilibrium is unstable and, if the E field intensity is high enough, the particle starts to rotate. The rotational axis is always perpendicular to $\vec{E}$. Figure taken from [13].

This effect has been studied widely for solid dielectric sphere particles, and the particle rotates around itself, with an axis pointing in any direction perpendicular to the electric field[13]. The angle the dipole is tilted, is increased with increasing field strength.

Unlike a solid particle, we know there is fluid flow even for small fields in a liquid drop, i.e. flow described by Taylors leaky dielectric model. So for higher fields we have a transition from leaky dielectric flow to rotational flow and leaky dielectric flow. The tilt angle of the droplet is defined as in figure 2.8. The drop

deformation caused by the Taylor flow component is constantly convected away by the rotational flow component, and thus limiting the total deformation of the drop. Hiromi Sato *et al.*(2006) observed different kinds of rotational motion for silicone drops in castor oil[14]. One similar to quincke, where the drop had an tilted deformation angle with respect to field direction, and another where the drops deformation oscillated between oblate and prolate shape. For their highest fields or drop sizes, drop break-up similar to type (3) break-up described by Allan and Mason were seen. Krause and Chandratreya(1998) have observed rotational motion similar to that of a solid particle[15], here the drops symmetric axis rotated.

Some studies have been made to determine the critical field strength, E_c, which needs to be exceeded to achieve rotation. For quincke rotation af a rigid sphere, the critical field is given as[2]

$$E_Q = \sqrt{\frac{2\sigma_{out}\eta_{out}(R+2)^2}{3\epsilon_{in}\epsilon_{out}(1-RS)}} \tag{2.25}$$

Feng(2002) came up with a electro-hydrodynamic model for the rotation in fluid drops. He included the charge convection in his EHD model, assumed negligible by Taylor in his leaky dielectric model. According to Feng, the critical field strength, could be described as[16]:

$$E_c = \sqrt{\frac{(\sigma_{out}+\sigma_{in})^2\epsilon_0\eta_{out}a}{(\sigma_{out}\epsilon_{in}-\sigma_{in}\epsilon_{out})\epsilon_{out}\gamma}} \tag{2.26}$$

Salipante and Vlahovska(2010) has shown experimentally that the critical field for when rotation occurs depends on fluid viscosity ratio and drop size, and that for small high viscosity drops, the rotation was similar to that of a solid dielectric sphere described by Quincke[2]. Increasing drop size and drop viscosity will reduce the critical field value, where the viscosity dependence is stronger. In addition, drop tilt angle gradually increases with increasing fields for high drop viscosities, while low viscosity drops suddenly transition into a large tilt angle.

For even higher fields, chaotic behavior can occur. An experiment by Lemaire and Lobry(2002) with a dielectric cylinder submerged in a weakly conductive fluid, showed constant angular velocity above the critical field strength required for quincke rotation. For even higher fields, the behavior was chaotic, the angular velocity was no longer constant and the rotation direction changed direction randomly.

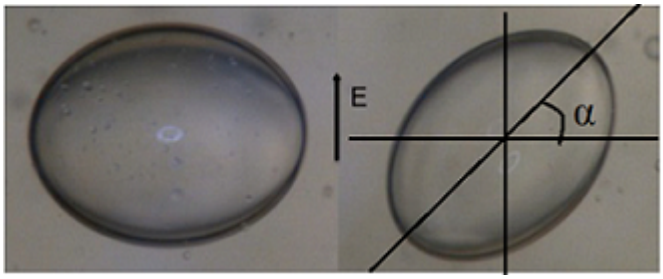

Figure 2.8: Figure showing tilt angle. Left side shows an oblate drop before the critical field strength have been reached. Right side shows the tilted drop for an electric field strength higher than the critical field strength. Figure adapted from [2].

2.7 Dielectrophoresis and Pickering emulsions

The fact that small particles have a tendency to get trapped at liquid-liquid or liquid-gas interfaces, was descovered by Ramsden in 1903, and later on by Pickering in 1907. When the particles get adsorbed at the interface, they reduce the unfavorable contact between the two immiscible fluids, and thus lowering the interfacial energy resulting in them getting trapped there[17]. Pickering recognized that the build up of particles on liquid drops, could hinder drop coalescence, and therefore be used as emulsion stabilizers[18].

When a dielectric particle is subjected to a non-uniform field, the particle experiences a force towards regions of higher or lower electric fields depending on the dielectric properties of the particle and the surrounding medium[19]. This phenomena is known as dielectrophoresis(DEP), and was first described by Pohl(1951), who concluded that particles with higher dielectric constant than its surrounding medium, will be attracted to regions with higher electric field, and vice versa. Also the DEP force wasn't dependent on field polarity, resulting in DEP ocurring in both DC and AC fields.

A drop in a uniform electric field, will distort the field around the drop, e.g. as seen in figure 2.1. This means that particles, as well as other drops, in a drops vicinity will be affected by DEP. For particles inside the drop, the DEP force is zero due to the uniform field inside the drop. Particles trapped on the drop-fluid interface will be affected as long as some of the particle is located outside of the drop.

A study by Hwang *et al.*(2010)[3] looked at the effects of DEP on drops with micrometer sized particles acting like that seen in Pickering emulsions. If we look at the particle as point dipoles submerged in a fluid, the DEP force acting on them can be found and was defined by Hwang *et al.* as

$$F_{DEP} = 2\pi R_p^3 \epsilon_0 \epsilon_{out} \beta'(\omega) \nabla E^2, \tag{2.27}$$

where R_p is the particle radius, E is the root-mean-squared value of the electric field in AC fields, and $\beta'(\omega)$ is the Clausius-Mossotti factor given as

$$\beta'(\omega) = Re\left(\frac{\epsilon_p^* - \epsilon_{out}^*}{\epsilon_p^* + 2\epsilon_{out}^*}\right) \tag{2.28}$$

where ϵ_p^* and ϵ_{out}^* are the frequency dependent complex permittivities of the particle and the surrounding fluid, respectively. The tangential force on a particle located on a drop-liquid interface was derived by Hwang *et al.* by assuming the drop stays spherical and that the electric field is only affected by the drop, not the particles. They found the tangential force to be:

$$F_{DEP,\theta} = -12\pi R_p^3 \frac{1}{a} \epsilon_0 \epsilon_{out} E_0^2 \beta' \beta (2+\beta) cos\theta sin\theta \tag{2.29}$$

where β is the Clausius-Mossotti factor for the drop and fluid given as

$$\beta(\omega) = Re\left(\frac{\epsilon_{in}^* - \epsilon_{out}^*}{\epsilon_{in}^* + 2\epsilon_{out}^*}\right) \tag{2.30}$$

where ϵ_{in}^* is the frequency dependent complex permittivity of the drop, and ϵ_{out}^* is the frequency dependent complex permittivity of the fluid as before.

From equation (2.29) we see that the force is zero at the poles and equator, and at its maximum at 45°. Also increasing drop size will reduce the DEP force. The direction of the force is from poles to equator for positive $F_{DEP,\theta}$, and from equator to poles for negative $F_{DEP,\theta}$. Since $\mid \beta \mid \leq 1$, the direction is decided by $\beta'\beta$, $\beta'\beta < 0$ gives a force from poles to equator while $\beta'\beta > 0$ gives a force from equator to poles.

In the experiments by Hwang *et al.* they used DEP to move the particles, thus destabilizing the Pickering emulsion by allowing drops to merge. Figure 2.9 shows an illustration for the two cases of negative and positive $\beta'\beta$.

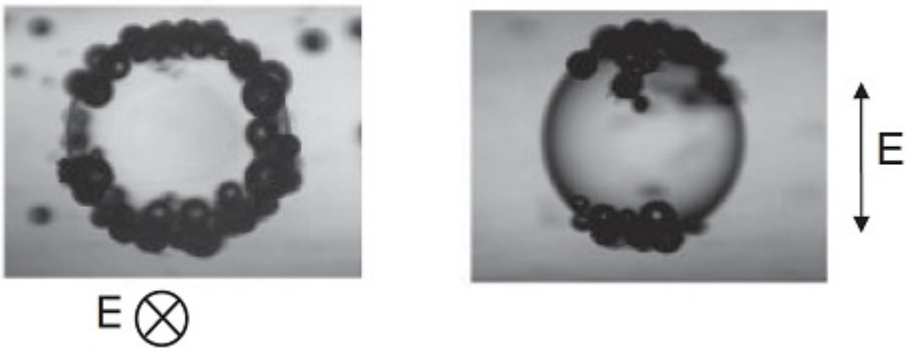

Figure 2.9: Shows two different cases of DEP force acting on Pickering particles. On the left, $\beta'\beta < 0$ and viewed parallel to field. On the right, $\beta'\beta > 0$ and viewed perpendicular to field. Figure adapted from [3].

Chapter 3

Clay and electrorheology

3.1 Clay

As said in the introduction, study of clay is the main theme in our research group. Clays may be viewed as good representative model systems for soft condensed matter and complex materials and is studied by incorporating clay into other synthetic and complex materials such as polymers, liquid crystals, colloids and bio materials[20].

The clay we've been working most with in this project is sodium-fluorohectorite. Na-Fh is a synthetic smectite clay, meaning it has a 2:1 molecular structure, with the empirical chemical formula $Na_{0.6}(Mg_{2.4}Li_{0.6})Si_4O_{10}F_2$ per half unit cell, where Na^+ is an interlayer exchangeable cation. The molecular crystal structure consists of three layers, two tetrahedral silica sheets, sandwiching one octahedral silica sheet, thus called a 2:1 clay. We've also been using Laponite clay, which also is a layered silicate which has the empirical chemical formula $Na^{0.7+}(Si_8Mg_{5.5}Li_{0.3}O_{20}(OH)_4)^{0.7-}$. The clays crystal structure forms 1 nm thick platelets with an average diameter of 30 nm, which stack together like cards. These stack of cards then again aggregates into larger grain particles, which we see as grains. In dry form the clay looks like white powder. The clay is polydispersed with grain sizes ranging from $\sim$100 nm to a few μm. An illustration of the clay structure for different scale sizes can be seen in figure 3.1.

Clay modified with cetyltrimethylammonium bromide, CTAB, with chemical formula $[CH_3(CH_2)_{15}]NBr(CH_3)_3$ has been shown to make the clay lipophilic

and thus disperse easier in oil compared to unmodified clay[21, 22]. This will result in smaller and more uniform clay particle aggregates and slower sedimentation over time. Illustration showing the slow sedimentation rate and improved oil dispersion of modified clay in silicone oil can be seen in figures 3.2 and 3.3.

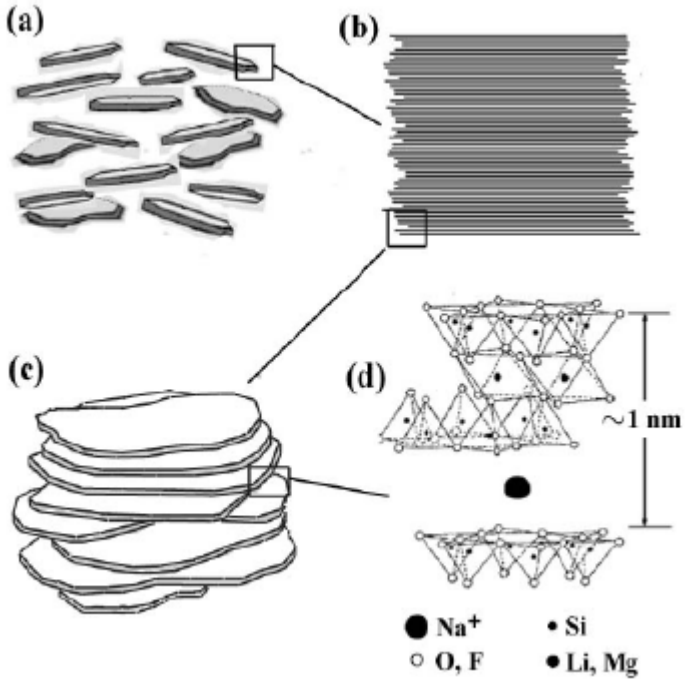

Figure 3.1: Illustration of smectite clay at different scales. (a) The clay looks like white powder when dry, and consists of aggregated stacks. (b) A single stack of platelets with size ∼100nm (c) Several platelets, each individual platelet has a crystal structure. (d) The crystal structure consists of three layers, two identical outer layers, and one middle layer, the crystal has a thickness of ∼1 nm.

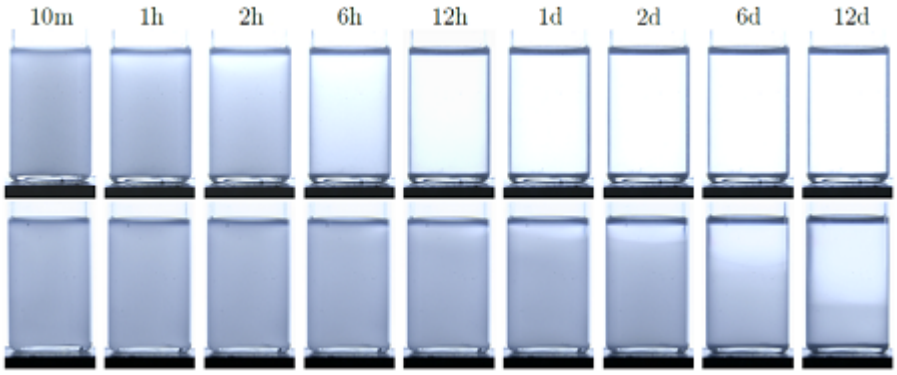

Figure 3.2: Shows the sedimentation rate of non-modified(top) vs modified clay(bottom) in silicone oil. From the left, photos are taken after 10 min, 1-2-6-12 hours and 1-2-6-12 days after mixing. Figure taken from [22].

3.2 Electrorheology

Our system consist of oil drops containing clay particles. So what really happens to the clay particles when we apply an electric field?

A study by Fossum *et al.*(2006)[23] investigated this showing fast and extended structuring of the clay particles. By applying a strong electric field, the clay particles formed chain formations, aligned along the electric field lines. For this to be understood the particles must be viewed as dipoles. This means the electric field induces electric dipoles in the clay particles, which have no dipole in zero field. X-ray scattering studies done by Fossum *et al.*, revealed that the particles polarize and align along the silica sheets. It was also noticed a change in the platelet separation, indicating that the intercalated ions, and possibly the water molecules play a role in the particle polarization process. When polarized, the particles reorients and form visible macroscopic chains. A photo of this kind of chain formation can be seen in figure 3.4. These chains will alter the rheological properties of the fluid containing the clay. Thus we can call the fluid mixed with clay an electrorheological fluid.

When it comes to the modified clay, the smaller and more uniform particle aggregates we get compared to non-modified clay, results in an overall better alignment of the clay particles when subjected to an electric field[21, 22].

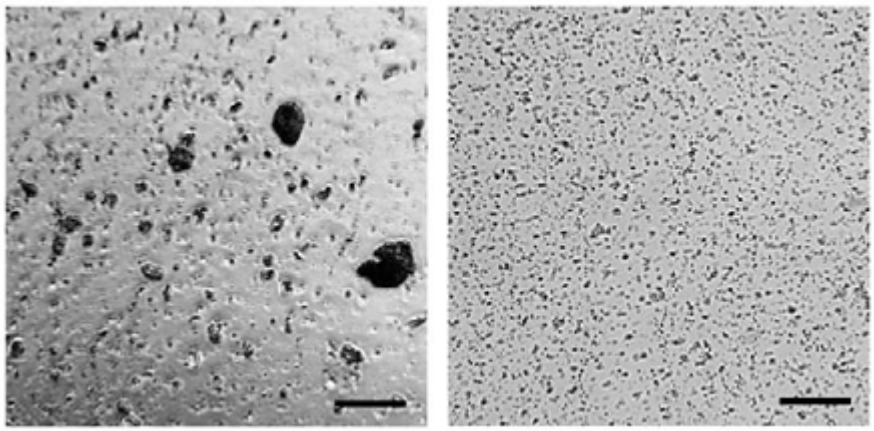

Figure 3.3: Shows the improved dispersion of modified clay(right) over non-modified clay(left) in silicone oil. The length of the bar corresponds to 200μm. Figure adapted from [22].

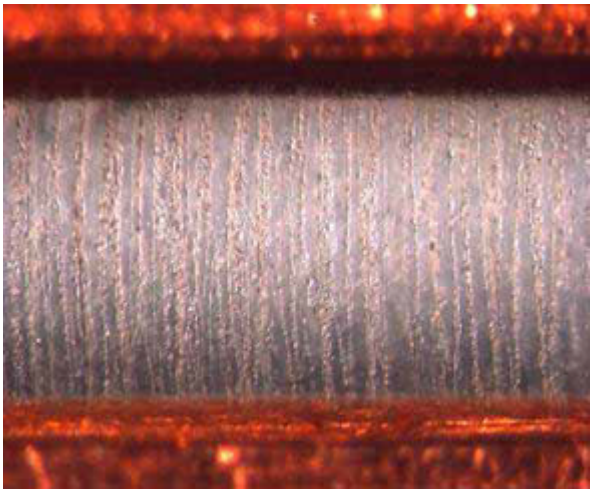

Figure 3.4: Photo of chain formation of clay particles between two Cu-electrodes when an electric field is applied.

Chapter 4

Experimental setup and procedure

4.1 Setup

The experimental setup is shown in figure 4.1. For DC signals we used a voltage generator and amplifier capable of delivering voltages up to ∼10 kV. For AC signals we used a script in the program MATLAB and a DAQ aquisition card connected to the computer to generate signals. Signals(Square AC) with a max peak-to-peak voltage of 20 V could be generated. Frequency and duration of the signal could also be adjusted. The generated AC signal was then amplified 300 times with a voltage amplifier before reaching the sample cell. Resulting in one electrode with the amplified AC signal, whilst the other one functioning as electric gound(earth). Both the generated signals and the amplified signals were monitored on an oscilloscope.

In order to view the droplet inside the sample cell a Sony HD video camera and a Canon HD photo camera(which also had the ability to record video) were used in addition to two microscopes and two light sources which lid up the sample cell from behind. The optical paths of the two cameras were normal to each other, enabling view both parallel and perpendicular to the electric field direction. To better visualize if the field was on or off(nescessary for low fields were fluid flow is hard to detect), a red LED were pointed towards the cell which lid up when the field was on. This way we could see a weak red light reflected from the droplet when the field was turned on in the recorded videos and photos,

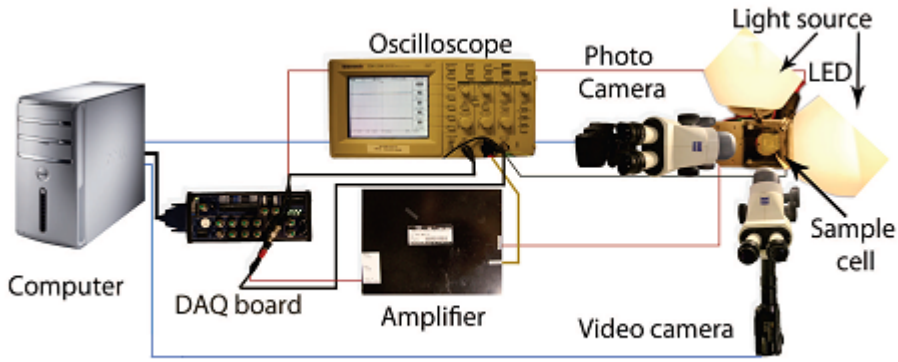

Figure 4.1: Illustration of the experimental setup.

giving us the exact time and duration of the field when analyzing the fluid and clay particle motion. Manual focus on the cameras along with manual focus on the microscopes and a adjustable stage supporting the sample cell were used to keep the drop in picture and focused.

4.2 Sample cell

The sample cells we used were custom made with cubic shape, ∼1 cm width and length, and ∼25 mm height. The cell was made out of two plexiglass walls and two ITO(Indium Tin Oxide) covered plexiglass walls. ITO is a transparent conducting material, and acted as the electrodes. Only one side of the electrodes were conductive, i.e. only one side covered with ITO. We used several cells for different experiments, where some cells had electrodes with their conductive side facing outwards, and some cells had electrodes facing inwards, so we could choose whether or not the electrodes would be in contact with the solution. The plexiglass has a high dielectric constant and works as a good electric insulator.

It has been shown that the electric field is not uniform accross the entire cell[14]. The field is uniform in the middle of the cell, that is a quarter of the total length towards each electrode from the middle plane of the cell. This means for our cells of ∼1 cm, we would have ∼5 mm of uniform field in the middle of the cell. This means drop sizes should be less than this to avoid any

unwanted influence from non-uniform fields. Since horizontal drop movement also occurs, drops should be even smaller than the uniform field zone, so that some movement can be tolerated and still keep the drop inside the uniform field.

The transparent electrodes enabled a view parallel to the electric field, which would not be possible if we used standard Cu-electrodes. In order to connect the electrode walls to the voltage amplifier, we used conducting tape(made out of Cu) attached to the walls, and crocodile clips. A photo of one of the sample cells is shown in figure 4.2.

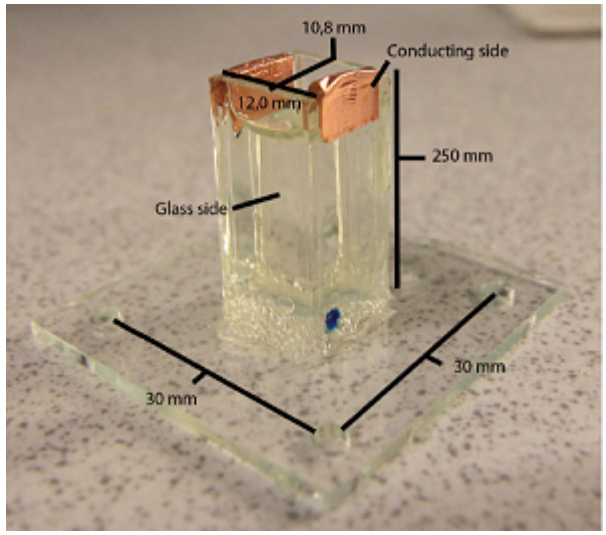

Figure 4.2: Photo of one of the sample cells, conducting Cu-tape attached to the conducting sides. There's a misprint in the height value of the cell, the real value is 25 mm.

4.3 Sample preparation

We used castor oil(Fluka 83912 delivered by Sigma-Aldrich Norway AS) as a suspending liquid and silicone oil(100 cSt from Dow Corning 200) as droplets. Silicone oil is immiscible with castor oil, so the two oils won't mix. The use of an organic oil, such as castor oil, for suspending liquid is desired since it has a conductivity $\sim$10 times higher than silicone oil. This criteria makes it

Table 4.1: Conductivity, dielectric constant and viscosity values for the two oils used. An estimated guess has been taken for the conductivity of 100 cSt silicone oil.

Oil	Conductivity σ (pS/m)	Dielectric constant ϵ	Viscosity η (cSt)
Silicone oil	∼3-5	2.13	100
Castor oil	45	3.37	800

easier to meet the requirements for oblate deformation and Quincke flow(which required $\tau_{in} < \tau_{out}$), which we wish to be able to observe. Silicone oil has a density of 0.965 kg/L and castor oil a density of 0.961 kg/L, and the high viscosity of the castor oil results in a slow sink rate of the silicone droplet, which is favorable due to not only making it easier to capture the droplet on camera, but also makes fluid motion due to fall speed negligible compared to the electrically induced fluid flow. The manufacture given viscosity, previosuly measured conductivity and dielectric constant values of the the two oils are given in table 4.1. Conductivity and dielectric constant values have previously been measured by a master student who was in our group, Kjetil Hersvik. He was only able to measure the conductivity of 10 cST Silicone oil, which scaled with the field, i.e. non-ohmic nature. The measures was 3 pS/m and 5 pS/m for 150 V/mm and 300 V/mm respectively, and its a reasonable estimate that the conductivity for 100 cSt Silicone oil lies in this regime too, since there's only a viscosity difference between the two. For our values of conductivity, dielectric constants and viscosity, we get $R \sim 0.07$, $S \sim 1.58$ and $M = 8$ for a sillicone drop in castor oil. In other articles the values have been similar to what we are using, except the dielectric constants seems to be larger, this don't change the ratio of S, but will affect the deformation calculation. Vizika *et al.* for example list ϵ_{out} as 4.45, and gives the interfacial tension between the two oils as $4.61 * 10^{-3}$ N/m[24].

The clay powder was pulverized using a pestle and mortar, except for the Laponite clay, which was already a very fine powder from the manufacturer. Then clay and silcone oil was measured and then mixed by a magnetic stirrer for at least 48 hours followed by putting the sample in an ultrasonic bath for at least half an hour before any experiments were done. Sufficient blending is nescessary to avoid that the clay aggregates into big particles. Samples ranging from 0.5 % to 5.0 % clay concentration by weight were made. The samples were labeled with their approximate concentration and clay type. The clay samples label and their actual concentration can be seen in table 4.2.

Table 4.2: Clay-oil samples made and their clay concentration.

Sample label	Weight Silicone oil(g)	Weight clay(g)	Concentration
0.5% Na-Fh	1.7845	0.0085	0.47%
1% Na-Fh	1.9074	0.0214	1.11%
1.5% Na-Fh	2.1325	0.0316	1.46%
2% Na-Fh	2.3225	0.0456	1.93%
2.5% Na-Fh	2.0550	0.0511	2.43%
3% Na-Fh	1.9731	0.0601	2.96%
4% Na-Fh	2.3351	0.0925	3.81%
5% Na-Fh	2.5575	0.1249	4.66%
0.5% 3CEC-FH	0.8628	0.0040	0.46%
1% 3CEC-FH	3.6543	0.0372	1.01%
1.5% 3CEC-FH	1.8013	0.0291	1.59%
1% Laponite RD	1.7523	0.0180	0.93%
1% Laponite S	1.9000	0.0190	0.99%
1% Rockwood	2.3986	0.0219	0.90%

After the silcone samples containing clay were ready, the sample cell was filled with castor oil, and then silicone drops were placed in the middle of the sample cell using a high performance pipettor with accuracy ± 0.1 μL. When the silicone droplet containing clay where in place, the field was turned on and the development were recorded using the cameras. When the electric field was on, the droplet could move move both horizontally and by sinking. So constant adjustment of the focus and the stage holding the sample cell had to be done. The time between the droplet is made to the field is turned on had to be kept as short as possible, since the clay particles would slowly sink to the bottom of the droplet and aggregate into larger particles if given to much time.

Several experiments were done to figure out what happens in a drop when clay particles are added, and how clay concentration, clay type and field strength have an effect on the results.

Chapter 5

Experimental results

5.1 Ring formation over time

The flow inside and outside a drop in a DC electric field will cause the clay to gather around the equator of the drop forming a ring-like(or ribbon-like) structure, as seen in picture 2.4. We now wished to see how both clay concentration and electric field strength would affect ring size and formation time.

The experiment was done by filming drops of different concentrations in different electric field strengths. For each experiment, five 2.5 μL drops($\sim$1.55 mm diameter) were made. Then the size of the ring (viewed perpendicular to the electric field), was calculated by measuring the pixel lengths from snapshots of the video for given times. The ring size is defined as ring width divided by drop diameter. The ring size was measured every 10 seconds and the average size for all 5 drops over time was plotted. The time error in plots are assumed to be the same as the frame rate in the videos, which is 25 frames per second, i.e. an error of $\frac{1}{25}$ seconds. This error is smaller than the plot point markers, so no errorbars for time are included in the plots. The error when measuring pixels have been estimated to 5 pixels, this is mainly due to uneven rings and/or focus issues in the video. Plots with pixel errorbars and standard deviation can be seen in appendix B.1, since often errors were smaller than the plot point markers or caused the plots to appear unclear. Figure 5.1 shows an example of how the ring formation and ring size increases over time. The figure shows video snapshots from the first minute of a 1 wt.% Na-Fh drop in a 200 V/mm field.

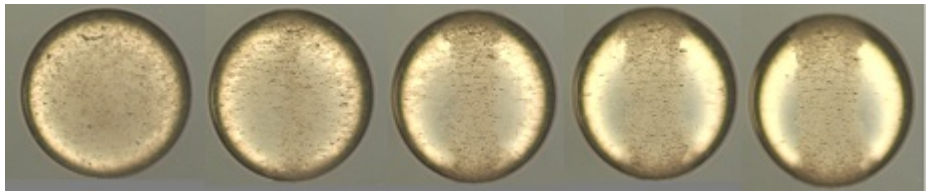

Figure 5.1: A photo series showing ring formation for a 1 wt.% Na-Fh drop in a 200 V/mm field over time. From left, the times are 0, 15, 30, 45 and 60 seconds respectively. Viewed perpendicular to the electric field. Drop radius ∼0.775 mm.

For Na-Fh, 0.5 wt.%, 1 wt.% and 1.5 wt.% concentration samples were tested in 100 V/mm and 200 V/mm fields. Ring formation was filmed for 180 seconds in 100 V/mm, and 120 seconds in 200 V/mm. The results can be seen in figure 5.2. The plot clearly shows how the ring size increases with increased clay concentration. One can also see that the ring formation happens faster in a 200 V/mm field than in a 100 V/mm field. Final ring size also seem to be dependent on field strength, except for 0.5 wt.% clay concentration, where there's little difference in the ring size for diferent field strengths. For 1.5 wt.% clay concentration it appears the ring size would keep on growing beyond the time limit set, so it's likely that the final ring width for 1.5 wt.% clay concentration is even higher than shown in the plot. Images showing the differences in ring size for different fields and concentrations can be seen in figure 5.3. Here we see drops with 0.5 wt.%, 1 wt.% and 1.5 wt.% Na-Fh after 3 min in a 100 V/mm and after 2 min in a 200 V/mm field. It can clearly be seen how the ring size increases with concentration, and with field strength except for the 0.5 wt.% sample.

The plot showing ring formation over time showed an average for several drops. A plot of individual drops containing 1 wt.% Na-Fh in 100 V/mm and 200 V/mm can be seen in figure 5.4. Here we can see that drops with the same concentration almost have the same kind of curve in the plot, but the ring size can variate some.

After testing clay concentrations and field strengths effect on the ring formation, different clay types were tested. By the same method as before, five drops of each clay type were put in a 200 V/mm field, and the average plotted. The different clay types tested were modified fluorohectorite(3CEC-Fh), Laponite RD, Laponite S and Rockwood modified Laponite in addition to Na-Fh. Re-

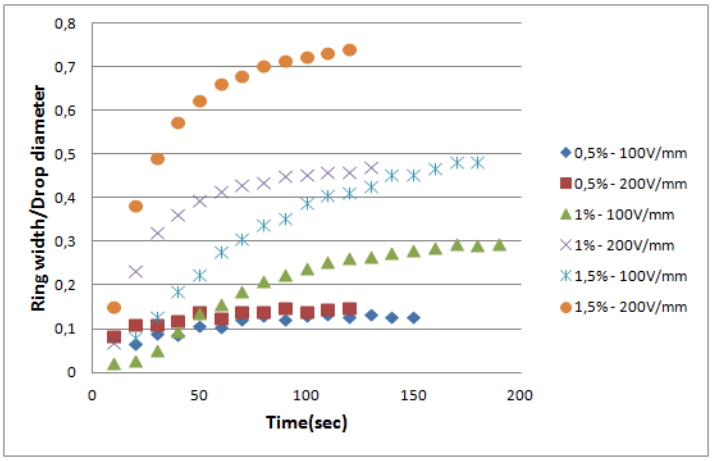

Figure 5.2: Plot showing ring size over time for drops with 0.5 wt.%, 1 wt.% and 1.5 wt.% concentrations of Na-Fh in 100 V/mm and 200 V/mm fields. Drop radius ∼0.775 mm.

sults are shown in figure 5.5. Due to the darkness of the Rockwood clay, it wasn't possible to see the ring formation for this clay type, and thus not showing in the plot. In figure 5.5 we see that Na-Fh, Laponite RD and Laponite S display similar behavior and end up with similar ring sizes. 3CEC-Fh however has a more linear plot curve and a larger ring size. Laponite RD and S had more even rings than Na-Fh, i.e. ring size was more uniform around the equator compared to Na-Fh. Comparison between a Na-Fh ring and a Laponite RD ring can be seen in figure 5.6. For 3CEC-Fh and Rockwood modified Laponite the ring was shifted towards the negative electrode(ground). More about the behavior of modified clay can be found in section 5.5.

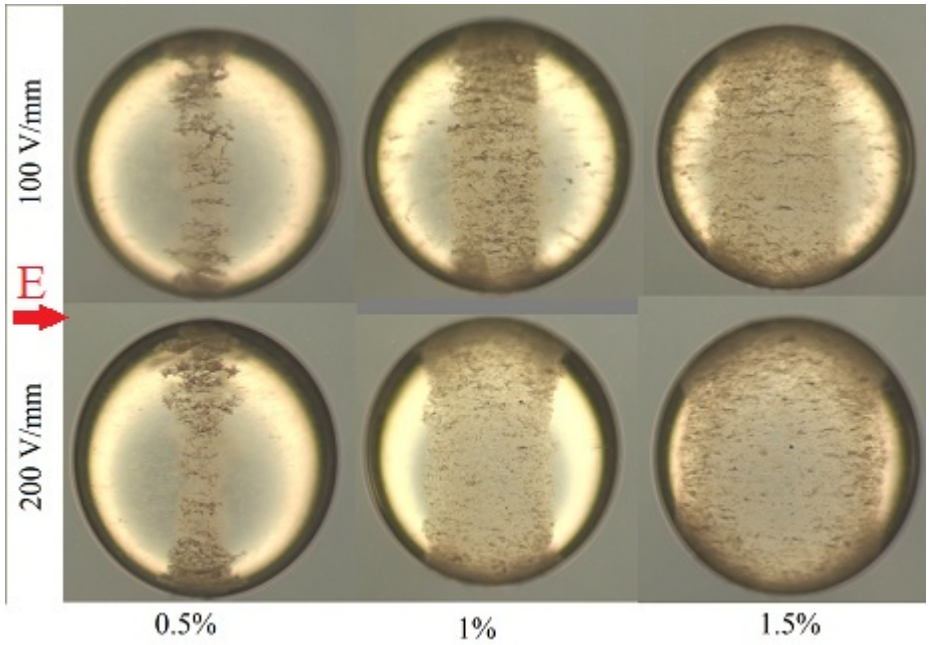

Figure 5.3: Photos showing ring size after 3 min in a 100 V/mm field(top), and after 2 min in a 200V/mm field(bottom). Concentration increases from the left. Drop radius ∼0.775 mm.

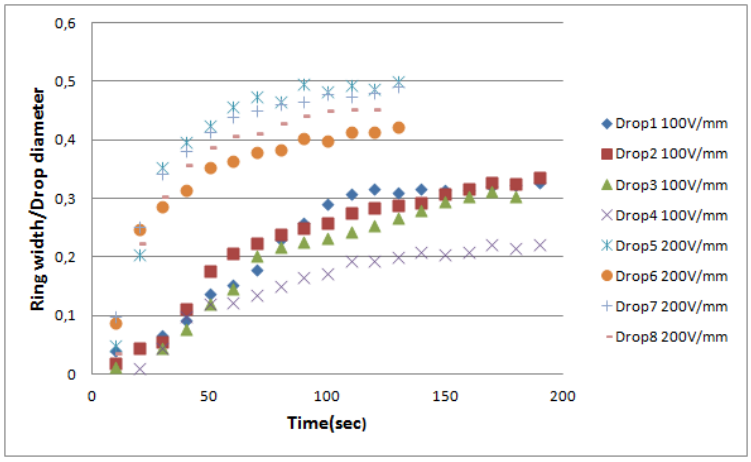

Figure 5.4: Plot showing ring size over time for individual drops with 1 wt.% concentrations of Na-Fh in 100 V/mm and 200 V/mm fields. Drop radius ∼0.775 mm.

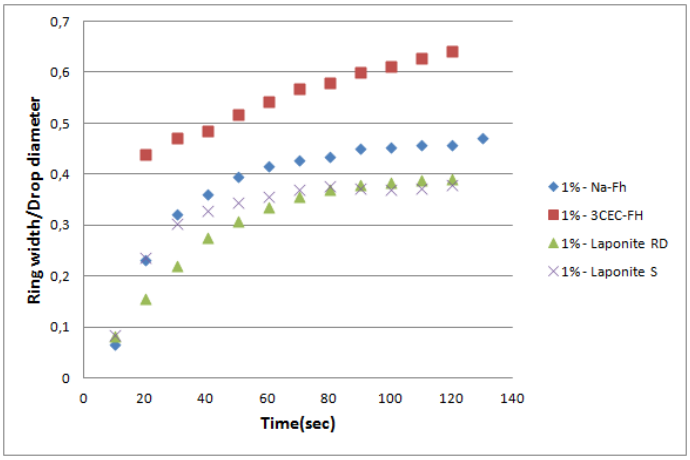

Figure 5.5: Plot showing ring size over time for drops with different types of clay in a 200 V/mm field. Due to the different formation of the ring for 3CEC-Fh, the ring size was difficult to measure after 10 seconds for this sample, so this meaurement is left out of the plot. Drop radius ∼0.775 mm.

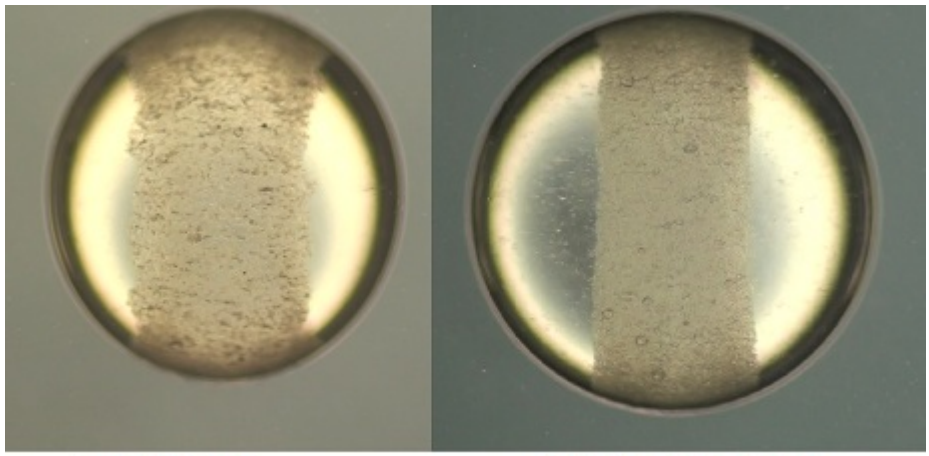

Figure 5.6: Photos of a Na-Fh ring compared to a Laponite RD ring in a 200 V/mm field. It can be seen that the Laponite RD ring has a much more even size around the equator. Drop radius ∼0.775 mm.

5.2 Antiring

We have now seen how the flow makes the clay gather as a ring around the drops equator. From equation (2.22) we can see that the flow is against the equator for a silicone drop in castor oil. We now wanted to see if we could get the clay to gather at the poles, i.e. reverse the flow. According to theory we can achieve this by simply putting a castor oil drop in a silicone suspending fluid instead. This will give v_θ a positive value, meaning the flow is reversed, flowing from the equator to the poles. It also results in lower velocity compared to when we had a silicone drop in castor oil. This means we would need a higher field to achieve the same velocities as in the original case. The electric field scaling factor is ∼4.5. For the experiments we therefore expected to see reversed flow in fields ∼450 V/mm to ∼900 V/mm with similar velocities as for the original case where we looked at fields 100 V/mm and 200 V/mm.

During the experiments however, we were unable to observe any flow, this was due to the low viscosity of the silicone suspending fluid, which resulting in the castor oil drops moving too fast horizontally due to the electric forces, and quickly hitting the eletrodes. Upon contact with the electrodes, the castor oil drops also bursted and laid out like a thin film across the electrodes. Even for for lower fields(<400 V/mm), no leaky dielectric flow was witnessed, just slower horizontal drop movement. A mixture of 100 cSt and 10000 cSt silicone oil was also made(∼600 cST) to increase the viscosity of the suspending fluid to prevent the horizontal movement. This will however according to equation (2.22) reduce v_θ even further. With the higher viscosity silicone oil, the drop didn't move as much horizontally, but no reversed flow was observed either, just prolate deformation and break-up of the castor oil drop in low fields(∼200 V/mm).

5.3 Clay chains

In an electric field, the clay polarizes and forms chains aligned with the field lines. The electric field inside a pure oil drop was given in the theory chapter as $V_{in} = \frac{3}{2+R}E_0$, where E_0 is the applied field. This will give a field $E_{in} \approx \frac{3}{2}E_0$ for a silicone oil drop suspended in castor oil, and a field $E_{in} \approx \frac{2}{10}E_0$ for a castor oil drop suspended in silicone oil. From this we can see that formation of clay chains should occur for lower fields in a silicone drop suspended in castor oil, than vice versa. Adding clay to the drop will however raise the conductivity of the drop, and thus lower the field some.

Since the castor oil drop experiments were unsuccesful, no chains could be seen for this case. For the silicone drops, clay chains were seen. In fact, the ring around the equator can be looked at as clay chains on top of each other. For low fields it was hard to see chain patterns, but it was clear that the clay particles attracted each other and stuck together once in contact with each other. For low clay concentrations, the electro-hydrodynamic flows dominated, and only a few small clay chains managed to form inside the drop before eventually ending up in the ring at the drop surface. For higher clay concentrations, more chains managed to form inside the drop, and as the concentration got higher, chain formation started to dominate over the electro-hydrodynamic flows, and prolate drop deformation happened instead of oblate deformation. By increasing the field, the ring size also increased as the chains were stretched out across the drop surface, making it easier to see the chain patterns. For high enough fields, the ring could be stretched across the entire drop. For high concentrations there was no ring, just the entire drop covered in clay. Images illustrating how the ring size increases and how chains appear more clearly in higher fields can be seen in figure 5.7. The figure also shows that the drop get a prolate deformation in the higher field. Another thing observed was that the shape of the drop

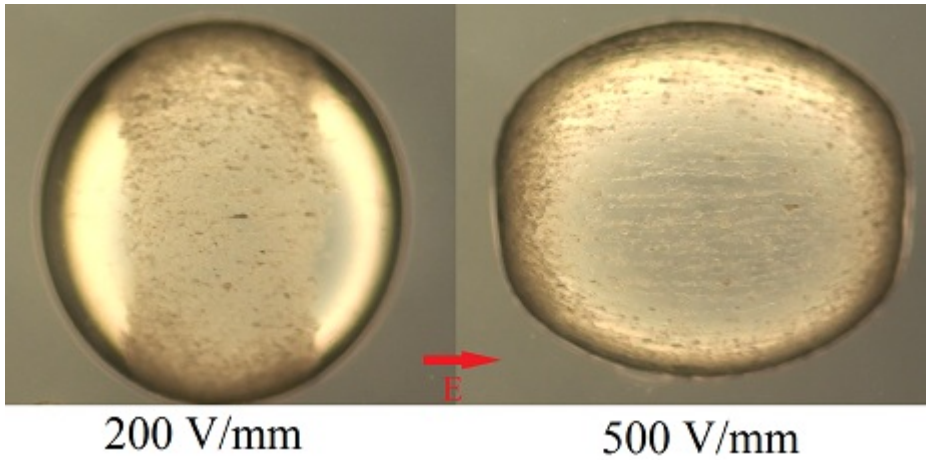

Figure 5.7: Photos showing how ring size increases and chains appear more clearly when the electric field is increased from 200 V/mm to 500 V/mm for a 1 wt.% Na-Fh silicone drop. Initial drop radius ∼0.775 mm.

deformation in high fields depended on how the field was applied. If a low field

was applied first(<200 V/mm), so that a narrow ring was formed, and then the field was increased, the drop would make a more square shape when deformed, compared to when the initial field was high, i.e. no ring formed at low field first, which would result in a more oval shaped deformation. An illustration of the oval and squared shape deformation can be seen in figure 5.8.

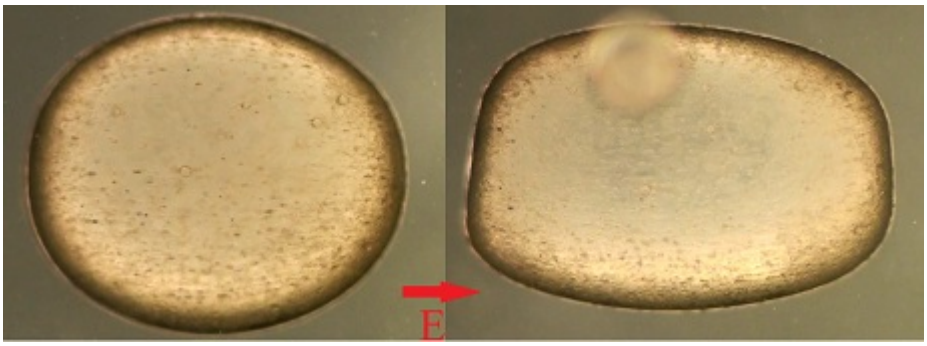

Figure 5.8: Deformations of a 1.5 wt.% Na-Fh drop. Left photo shows oval prolate deformation when a 500 V/mm field is applied. Right photo shows square prolate deformation after letting a ring form in a 200 V/mm field first and then increasing the field to 500 V/mm. A small drop stuck on cell wall can be seen out of focus in the right picture. Initial drop radius ∼0.775 mm.

5.4 AC field

Last semester we observed chains for drops in AC fields too. These chains were only seen inside the drop, and no ring was formed. The frequency used then was 200 Hz. We discussed alternating fields in section 2.3. Here we saw that by lowering the frequency below the Maxwell time, we should be able to achieve flow patterns just like those seen in a DC electric field. The alternating field direction should not affect the flow direction since it is dependent on E^2. The test were done on 2.5μL 1 wt.% Na-Fh drops with 100-300 V/mm AC fields. The test showed the drops deformation oscillating with the same frequency as the signal for low frequncies. The oscillation was the drop going from no deformation, to a slightly oblate deformation. The signal was square AC, however, the drop dropped back to no deformation and flow processes stopped each time the field alternated, and it took $\sim$1 second to gain full oblate deformation again and for the flow to reach maximum speed again. The drop deformation oscillation could be seen up to $\sim$3 Hz. Rings around the drop was observed up to $\sim$0.25 Hz. Photos of ring formation for different frequencies can be seen in figure 5.9. In the figure we can see how the ring formation increases with decreasing frequency. When the frequency increases, more and more chains throughout the drop appear instead of ring formation.

Another experiment was done where a cell filled with castor oil mixed with clay was put in a 300 V/mm AC field(Maximum for our AC amplifier). This caused the clay particles to form what appeared as weak chains between the two electrodes. Then a pure silicone drop was inserted in the cell. No big difference was observed. The the same experiment was done, only now with a 300 V/mm DC field. This time, the chains were easier to see and the added drop created flow which then again caused the chains near the drop to move and break up.

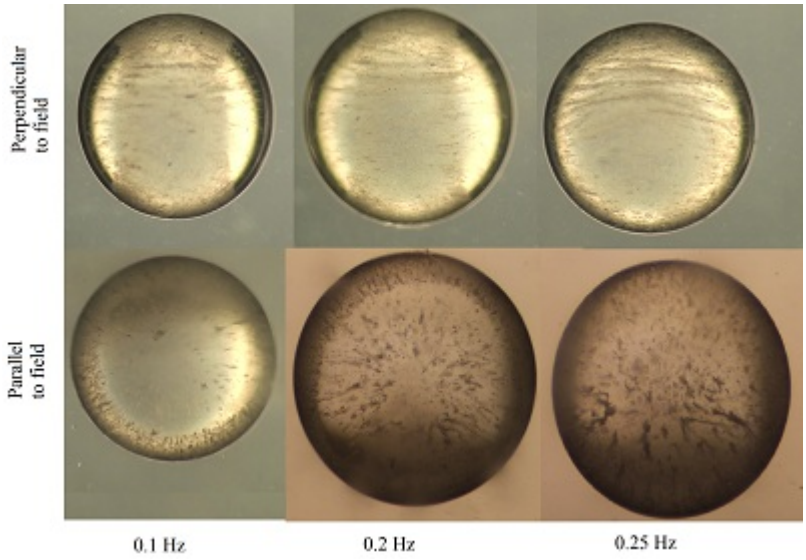

Figure 5.9: Shows ring formation after 3 min in a 150 V/mm AC field for different frequencies. Pictures on top are viewed perpendicular to electric field, pictures on bottom shows a parallel view to the elecric field. Color differences are due to different camera settings. Drop radius $\sim$0.775 mm.

5.5 Modified clay

The different behavior for modified clay in the ring measurement experiments, lead to some more tests. We've already seen that 3CEC-Fh had a wider ring than Na-Fh for 1 wt.% concentration for 100-200 V/mm fields. So we tested 0.5 wt.% and 1.5 wt.% 3CEC-Fh also. For 0.5 wt.% we didn't get a ring, but got a few chains on the drop surface instead. The flow still appeared to be similar to leaky dielectric flow. For 1.5 wt.% the flow appeared to stop after ∼10 seconds, when all of the drop surface was covered with clay particles, and chains were clearly visible. In addition we got prolate deformation. Inside the drop a few remaining clay particles bounced back and forth between the drop poles parallel to the electric field. Figure 5.11 compares the clay formation for 0.5 wt.% and 1.5 wt.% 3CEC-Fh and Na-Fh. For the 1 wt.% drops, the ring wasn't centered around the equator of the drop either, the clay formed at the pole facing the negative elecrode(ground), forming a hemisphere instead of a ring. This hemisphere behavior was also seen for Rockwood modified Laponite. The flow for the 1 wt.% case still seemed to be leaky dielectric flow. As the hemisphere was formed, the drop started to move against the field, towards the positive electrode. Examples of these hemispheres can be seen in figure 5.10.

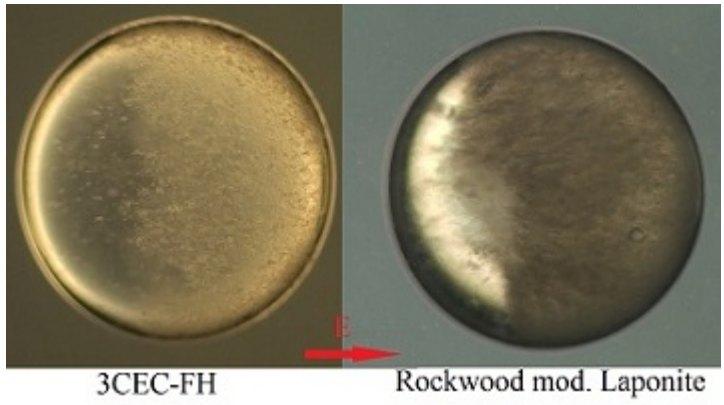

Figure 5.10: Photos showing the clay hemispheres for 3CEC-Fh(left) and Rockwood modified Laponite(right). The hemispheres forms on the drop pole facing the negative electrode(ground). When the hemispheres were formed, the drop started to move against the positive electrode. The different background colors are caused by different camera settings. Drop radius ∼0.775 mm.

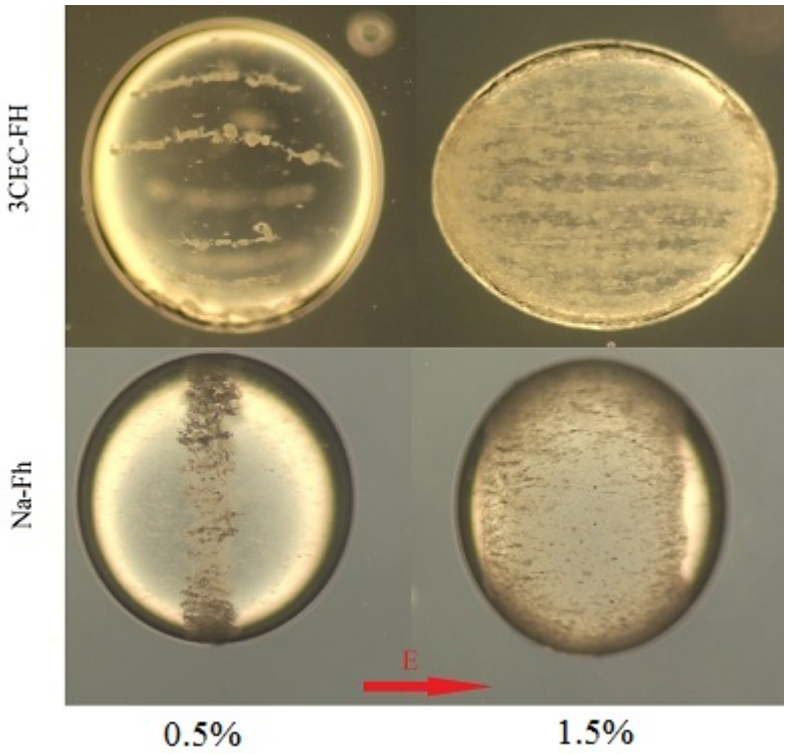

Figure 5.11: Photos comparing clay formation for drops with 3CEC-Fh and Na-Fh clay in a 200 V/mm field. 3CEC-Fh shown on top, while Na-Fh on bottom. For 0.5 wt.% one can clearly see the formation of a few long chains in the 3CEC-Fh drop, instead of the ring seen for the Na-Fh drop. For 1.5 wt.% 3CEC-Fh, the ring is streched across the entire drop and gives more visible chains, and a prolate deformation. The different background colors are caused by different camera settings. Initial drop radius ∼0.775 mm.

5.6 Field strength and concentration

To get a better understanding of the effects of field strength and clay concentration, drops with 0-5 wt.% Na-Fh concentration were tested in field strengths from 50 V/mm up to 640 V/mm. Three 2.5 μL drops for each concentration and field strength was tested. The results can be seen in figure 5.12 showing a phase diagram over the different drop behavior for different clay concentrations and field strengths. In the phase diagram we can see that for pure silicone

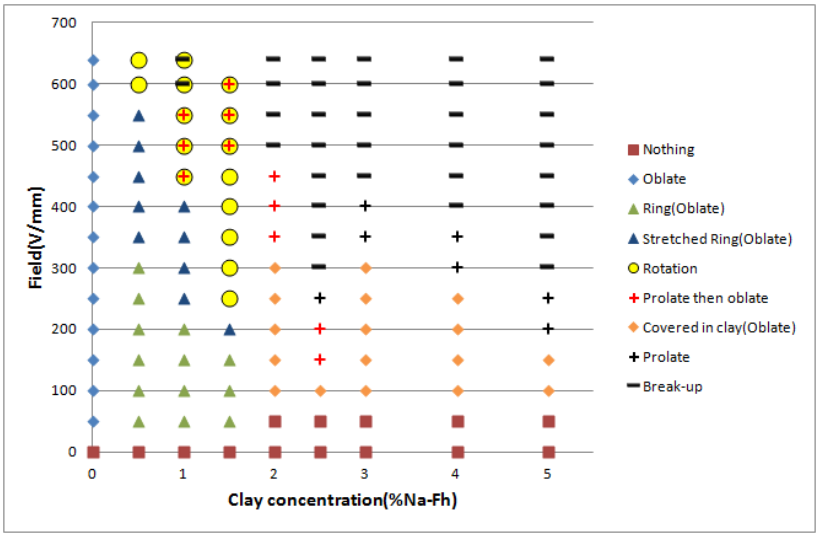

Figure 5.12: A phase diagram showing the different drop behavior for drops with Na-Fh clay for different clay concentrations and field strengths. Drop radius ~0.775 mm.

drops, only oblate deformation was observed. For 0.5 wt.% clay concentration, we see that low fields forms rings, and as the field increases the ring gets wider and stretched, i.e. cleary visible clay chains over the drop surface, and for high fields(>550 V/mm) drop rotation is observed. For 1 wt.% we see similar behavior as for 0.5 wt.%, only ring stretching and rotation happen for lower field values. For 450-550 V/mm the drop gets a prolate deformation initially when the field is turned on, but then the prolate deformation reduces over time, and the drop eventually ends up oblate, and finally the drop starts rotating. In addition we see drop break-up for fields 600-640 V/mm, where rotation occurs

for the broken up drops some time after break-up, given they didn't come in contact with electrodes during or after the break-up. 1.5 wt.% drops behave like 1 wt.% drops, except rotation occurs for lower field values, but initial prolate deformation requires higher fields compared to 1 wt.%, and no break-up is seen. The mark for 640 V/mm is left out, due to all the drops hitting the electrodes after a short time, but it looked to behave the same way as in 600 V/mm, except for sligthly larger initial prolate deformation. For 2-2.5 wt.% we no longer see any rotation, and the fields required for initial prolate deformation and drop break-up are lowered. For the lowest field values nothing much happens, electro-hydrodynamic flow stops early($<\sim$10 seconds), the drop is completely covered in clay and some clay particles bounce back and forth between the poles inside the drop. For 3 wt.% and above it looked like electro-hydrodynamic flow stopped early($<\sim$10 seconds), and the drop was covered in clay. Clay chains throughout the drop in addition to clay particle bouncing between the poles were also seen. The required field strengths for deformation and break-up was lowered as concentration increased in addition to the deformation staying prolate, instead of reducing over time like seen in the lower concentration drops.

5.7 Rotation

In figure 5.12 we can see we have drop rotation for high enough fields. For pure silicone drops rotation have also been seen, at fields of $\sim$1000 V/mm. For the pure silicone drop, a clear change in drop behavior occurs when the rotation starts. The drops deformation suddenly increases and tilts, and we can immediately see that the rotational flow starts. The entire drop and the nearby surrounding fluid rotates. The rotational axis seems to always be perpendicular to the electric field. In figure 5.13 an illustration of rotation for a pure silicone drop can be seen.

For drops containing 0.5 wt.% the rotation appear more chaotic. For this case there seem to be several vortices on the drop surface rotating in addition to leaky dielectric flow on the outside of the drop. The number of vortices and their rotational direction varies. During this chaotic rotation the drop stays oblate. If a ring is created first in a lower field, e.g. 200 V/mm, the vortices will cause the ring the bend back and forth like a snake. If a high field is applied initially, the vortices seems placed more chaotically, and changes in number and position over time. Phote of the 'snake'-like ring can be seen in figure 5.14.

For 1 wt.% and 1.5 wt.% drops, the drops have quincke like rotation again like pure silicone drops. For the 1 wt.% drops, the tilt can be seen for all fields

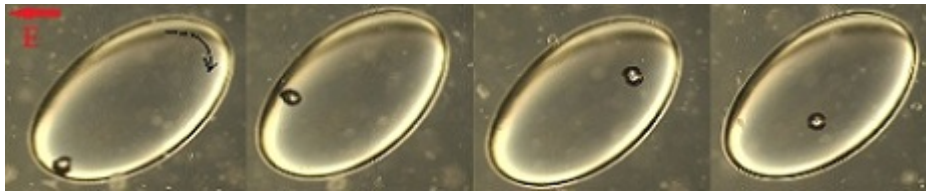

Figure 5.13: Shows tilt and rotation for a pure silicone drop in a 1000 V/mm field. The sequence last for ∼3 seconds. The rotation direction is indicated by the black curved arrow in the far left photo, but can also be seen from the little air bubble trapped inside the drop. As time goes by, from left to right, you can see the air bubble following a clockwise rotational pattern. Initial drop radius ∼0.775 mm.

rotation occurs, and for the 1.5 wt.% drops, the tilt seem to be minimal above 450 V/mm. The rotation occurs after a while, when the drop surface is almost completely covered in clay, often only one of the poles are clay free when the rotation starts. The rotational axis and the rotation have in some cases been observed to change direction over time. Pictures of rotating drops for 1 wt.% and 1.5 wt.% concentration can be seen in figure 5.15.

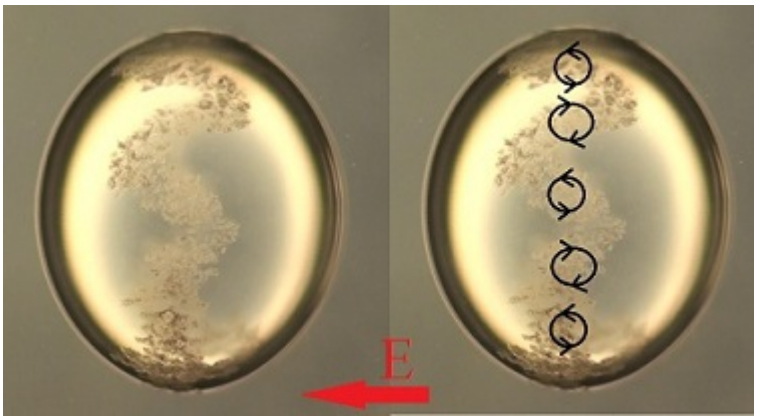

Figure 5.14: Photo of the 'snake'-like ring in a 600 V/mm field for a 0.5 wt.% Na-Fh drop. A ring had been made first in a 200 V/mm field. On the right the direction and position of the vortices have been drawn in. Initial drop radius ∼0.775 mm.

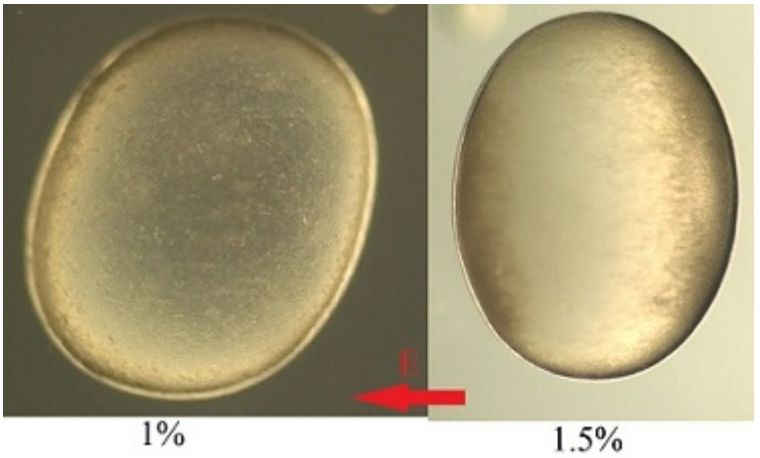

Figure 5.15: Photos of rotating drops with 1 wt.% Na-Fh(left), and 1.5% Na-Fh(right) in a 550 V/mm field. For the 1 wt.% case we can see the tilt in addition to the oblate deformation. For the 1.5 wt.% case no tilt is seen. Both drops are rotating clockwise with the rotational axis pointing upwards in the picture. Initial drop radius ∼0.775 mm.

5.8 Deformation and break-up

In the phase diagram, figure 5.12, we can see we have deformations for all clay concentrations, and as already mentioned, the deformation was dependent on time except for the pure silicone drops. To find out more about the deformations we recorded the average deformation over time for three 2.5 μL drops for each concentration of Na-Fh and field strength. A script in MATLAB was used to analyze snapshots from videos, and calculate the drop deformation. This was done by anlyzing pixel colors, and finding the biggest particle with similar colors in the picture. An example of a analyzed snapshot can be seen in figure 5.16 where the deformation calculated by MATLAB is drawn in. For pure silicone drops, this worked great. But for the clay drops it got harder to isolate the drop as the biggest particle and get its correct shape. This was caused by the difference in color between clay, drop and background. So for these cases the deformation was calculated by measuring the drop size by the pixels in the photo, just the same way ring size was measured. The error in pixel and time are assumed to be the same as before. This and very equal deformation for each individual drop, resulted in deformation error and standard deviation smaller than the plot point markers, so the errorbars are removed from the plots just like the time error.

The pure silicone drops almost instantly got to maximum deformation and the 0.5 wt.% drops the deformation did not change much over time. So the plotted deformation values of 0.5 wt.% drops, are all taken 1 min after field has been applied. The results can be seen in figure 5.17. As we can see oblate deformation increases with field strength except at 550 V/mm for the 0.5 wt.% drop, here the oblate deformation reduces. At 600 V/mm the 0.5 wt.% drop is rotating and the oblate deformation is increased again. The pure silicone drop also has a steady increase in oblate deformation, and then a major increase in deformation from 900 to 980 V/mm where we have quincke rotation.

For the rest of the deformation calculations, average deformation have been measured at 5, 10 and then every 10 seconds. For drops with 1 wt.% and 1.5 wt.% Na-Fh, we saw an early prolate deformation for high fields, which slowly reduced over time, and finally ended up oblate. Results can be seen plotted in figure 5.18. For the 1 wt.% drops a large initial prolate deformation was seen, as much as $\sim$0.67 for a 590 V/mm field. Even though all drops started prolate, they often ended up more oblate than the pure and 0.5 wt.% Na-Fh silicone drops as can be seen in figure 5.19. Illustration of the initial prolate drop deformation can be seen in figure 5.20. During this prolate deformation period, the clay particles covers the drop surface, and clay particle bouncing

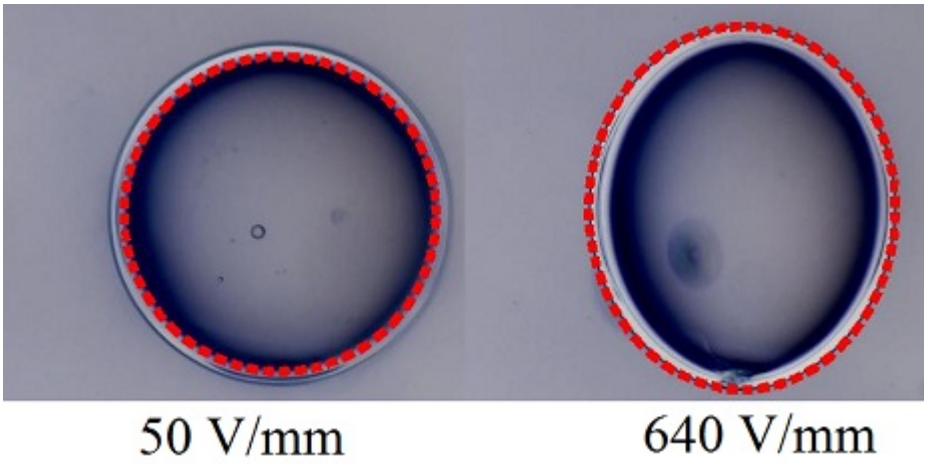

Figure 5.16: Photos analyzed in MATLAB of pure silicone drops in 50 V/mm and 640 V/mm fields. The calculated deformation is drawn in as a red dotted ellipse. Initial drop radius ∼0.775 mm.

between the poles could be seen inside the drop.

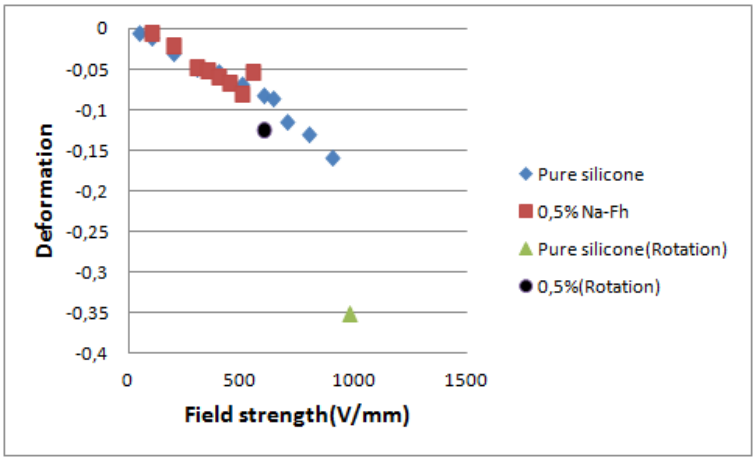

Figure 5.17: Plot showing deformation after 1 min for pure and 0.5 wt.% Na-Fh silicone drops. Initial drop radius ∼0.775 mm.

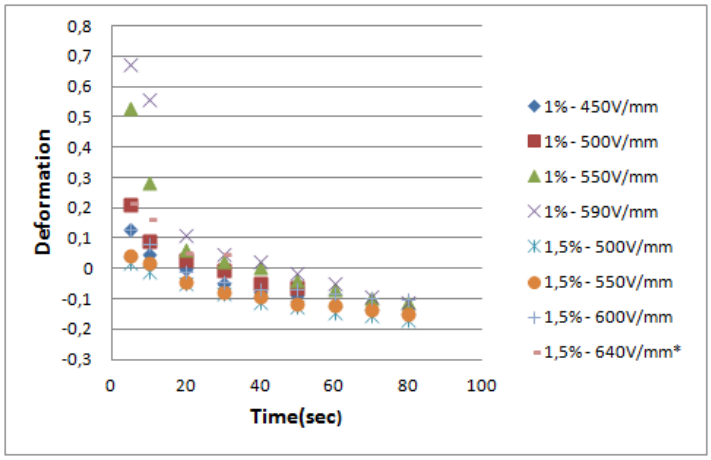

Figure 5.18: Plot showing deformation over time for 1 wt.% and 1.5 wt.% Na-Fh drops. ∗For 1.5 wt.% at 640 V/mm all drops hit electrodes after ∼30 seconds. Initial drop radius ∼0.775 mm.

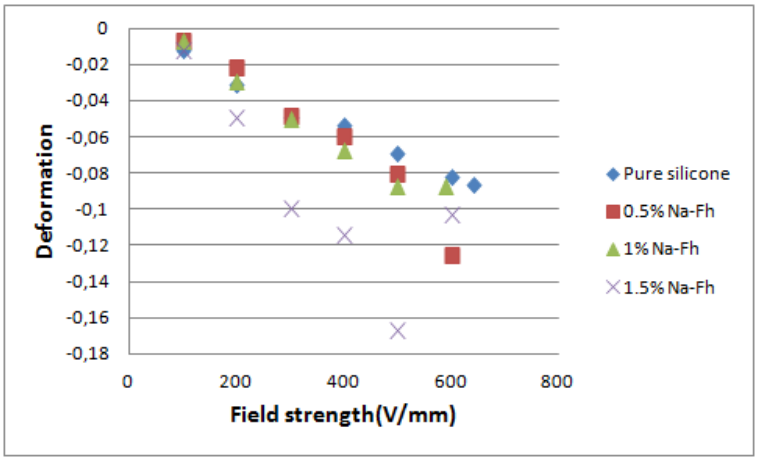

Figure 5.19: Plot comparing end oblate deformation for 0.5 wt.%, 1 wt.% and 1.5 wt.% Na-Fh drops to pure silicone drops for relevant fields. In fields where rotation occurred, deformation was measured before rotation started. Initial drop radius ∼0.775 mm.

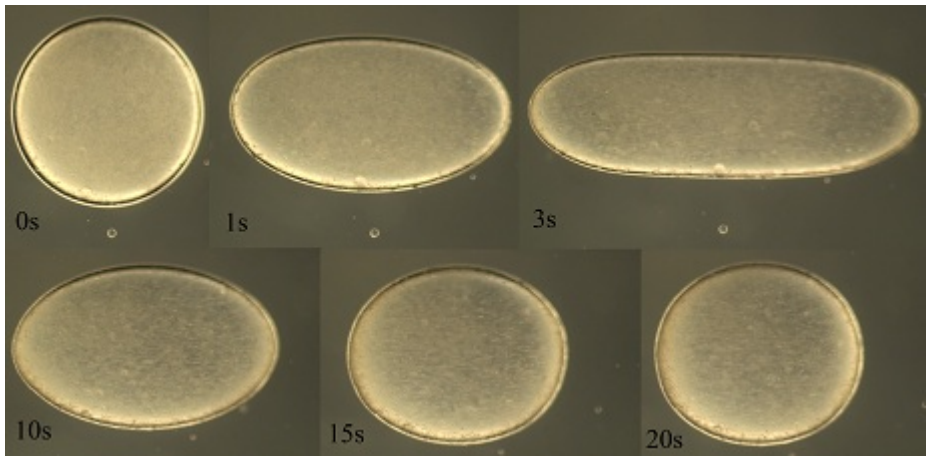

Figure 5.20: Photos illustrating the development of initial prolate deformation for a 1 wt.% Na-Fh drop in a 550 V/mm field. The time the field has been applied is shown. Viewed perpendicular to electric field. Initial drop radius ∼0.775 mm.

For 2 wt.% and 2.5 wt.% Na-Fh drops the initial prolate deformation happened for even lower fields than for the 1 wt.% and 1.5 wt.% case. The initial prolate deformation also happen over a longer period of time. The largest initial deformation without break-up of all clay concentrations and fields, were seen for the 2 wt.% drop in a 494 V/mm field with a deformation of ∼0.73. The 2.5 wt.% sample barely ends up oblate in 200 V/mm, and stays slightly prolate in 250 V/mm. Plot showing the deformation over time for 2 wt.% and 2.5 wt.% is shown in figure 5.21. For these concentrations the clay also covered the drop surface and clay particle bouncing was seen inside the drop.

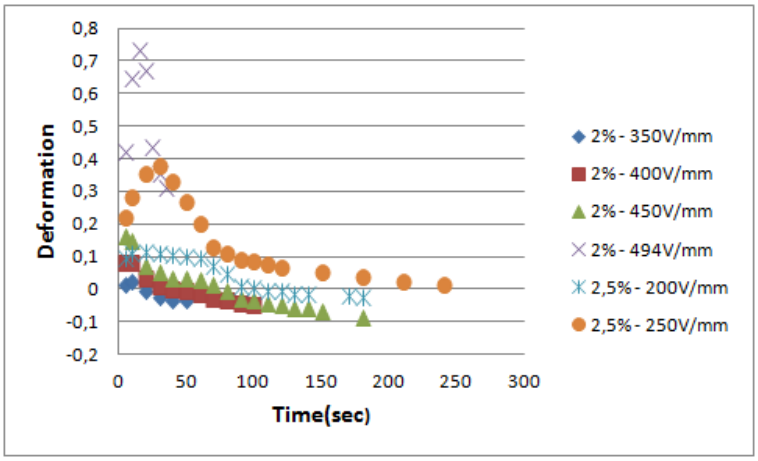

Figure 5.21: Plot showing deformation over time for 2 wt.% and 2.5 wt.% Na-Fh drops. Initial drop radius ∼0.775 mm.

For 3 wt.% and above drops had no deformation, time independent prolate deformation or increasing prolate deformation over time depending on field strength. Results are shown in figure 5.22. From the plot one can see the different concentrations behave similar to each other, but higher concentrations requires lower fields to achieve the same behavior. For 3 wt.% you could see clay particle bouncing inside the drop in addition to what appeared as chains. For 4 wt.% and 5 wt.% there seemed to only be stationary chains inside the drop.

For the highest fields we saw break-up of the drops for almost every concentration. When break-up was encountered, more test were done to find the critical field value for each concentration were break-up happened. This was

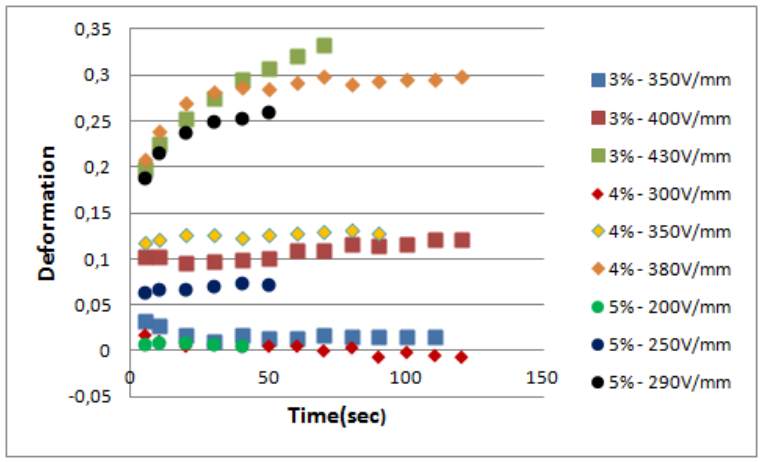

Figure 5.22: Plot showing deformation over time for 3 wt.%, 4 wt.% and 5 wt.% Na-Fh drops. Initial drop radius ∼0.775 mm.

done by testing testing more drops in the field range between observed break-up and previously non-break-up. Break-up happened in two different ways. One way was the drop simply breaking up into two or more drops. Another way the drop broke-up, was by stretching across the entire cell, and forming a bridge between the two electrodes. Eventually flows in the cell would brake the bridge, but the bridge usually lasted for several minutes. When the bridge broke it sometimes formed a chain of smaller drops still connecting the two electrodes, or the flow was strong enough to brake the connection alltogether resulting in several drops spread out in the cell. Illustrations of break-up and bridging can be seen in figures 5.24 and 5.23, respectively. The critical field values for break-up and bridging can be seen in table 5.1. From this we can see that for low concentrations, break-up happens at high fields, but as the concentration increases, bridging is more likely to occur. For 1.5 wt.% no break-up or bridging were seen. For 4 wt.% and 5 wt.% only bridging were seen.

Most of our experiments have been performed with fields up to 650 V/mm. Some experiments in higher field strengths were done for pure silicone, 0.5 wt.% and 1 wt.% Na-Fh drops. One obsevation for higher electric fields was another type of break-up, which could be more described as drop collapsing. For these high fields it has been observed that the drop stops rotating, and the poles of the drop gets pushed into the drop, and eventually tunneling through the drop,

Table 5.1: Critical field values for when break-up and bridging occurs for different Na-Fh concentrations. Initial drop radius ∼0.775 mm.

Concentration	Break-up(V/mm)	Bridging(V/mm)
1 wt.% Na-Fh	600	-
1.5 wt.% Na-Fh	-	-
2 wt.% Na-Fh	495	500
2.5 wt.% Na-Fh	255	270
3 wt.% Na-Fh	440	450
4 wt.% Na-Fh	-	390
5 wt.% Na-Fh	-	300

this often causes castor oil to get stuck inside the silicone drop. In these high fields(>650 V/mm), the electric field strength was gradually increased from 0 V. By doing this we didn't see the large initial deformation for the 1 wt.% drops which was that was observed if the applied field initially was high($\geq$ 450 V/mm). Illustration of the effect can be seen in figure 5.25.

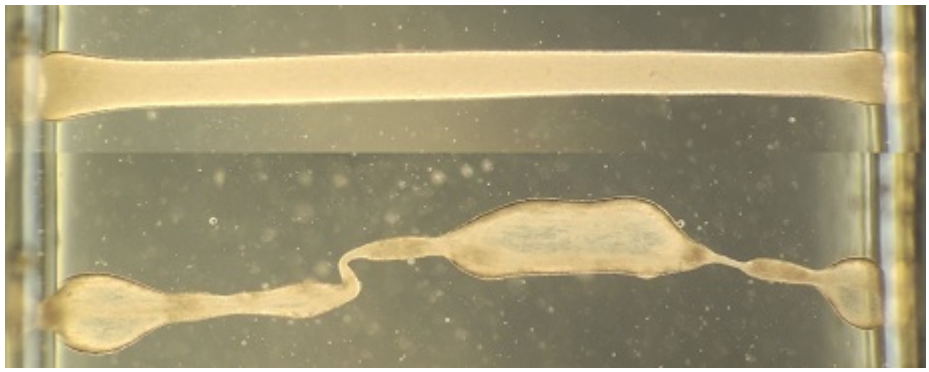

Figure 5.23: Shows a 4 wt.% Na-Fh drop making a bridge in a 500 V/mm field after 10 seconds(top) and 3 min(bottom). Initial drop radius ∼0.775 mm.

Figure 5.24: Shows an example of drop break-up for a 1 wt.% Na-Fh drop in a 640 V/mm field. One of the remaining drops started rotating after a while. The other one hit the electrode wall. Electric field direction towards the left in picture. Initial drop radius ∼0.775 mm.

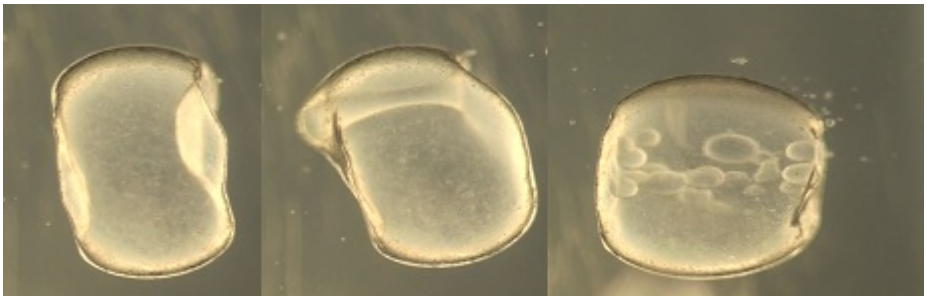

Figure 5.25: Shows the development of a collapsing 1 wt.% Na-Fh drop in a 800 V/mm field. On the left we can see the poles being forced into the drop. In the middle a tunnel between the poles have occurred. To the right the tunnel breaks, leaving small castor oil drops inside the larger silicone drop. The castor oil drops bounce back and forth into each other between the poles. Initial drop radius $\sim$0.775 mm.

5.9 Reversibility and settling

If a process is reversible or not can be useful for many applications. For our drops some of the processes are reversible, and some are not. This was studied by increasing, lowering and turning field off and on for the different drops. Letting the drop settle a long time before any field was turned on, and inbetween fields was also tested.

Ring formation is irreversible, meaning that when the clay has reached the drop surface, it stays there. The same was the case for when clay covered the entire drop. Letting the drop settle in no field after ring had been made, resulted in the clay particles falling downwards due to gravity, but not more than that you still clearly could see a ring. When turning the field back on, the ring went back to its original form. Stretching of the ring(chains) by increasing the field however is reversible, so you can stretch the ring and go back to smaller ring again, by increasing and lowering the field strength.

To make a drop rotate, its required to have a field applied for quite some time before the rotation starts. For example, the 1 wt.% Na-Fh drop in a 550 V/mm field initially get a prolate deformation, then slowly going to an oblate deformation, and then the rotation occurs, $\sim$90 seconds after the field was first applied. But when a rotation already have started, you could turn off the field, and the roation would resume right away if the field was turned back on again. It was also possible to make drops rotate for lower fields if one made a drop rotate in a high field first. This way rotation could to some degree be controlled by field strength.

The initial prolate deformation seen for drops with 1-2.5 wt.% clay concentration was just a one time occurrence. Turning the field off and on again after this initial deformation, didn't make the drop prolate again, just went back to the shape it had before the field was turned off. The same was true for the constant and increasing prolate deformed drops for high clay concentration(3-5 wt.%). The deformation could also be increased or lowered, by increasing or lowering the field.

The settling speed of drops where affected by rotation and deformation too. The majority of rotating drops didn't fall at all. Prolate deformations lowered the settling speed too, the largest prolate deformations almost made the drop stay stationary.

The main focus in this study was on single drops, but a few experiments trying to reverse break-up, i.e. merge broken up drops where done. Pure silicone drops and drops with low concentration had a tendency to attract each other in an electric field if placed close to each other. By increasing the field strength

high enough you could get drops to merge. For higher concentration drops(>3 wt.%), prolate deformation could cause drops far appart to merge, given that they where horizontally lined up along the field direction before field was turned on.

Chapter 6

Results and Discussion

6.1 The ring

From video analysis it can be seen that the electro-hydrodynamic flow inside and outside the drop clearly resembles what Taylor described in his leaky dielectric model for drops with low clay concentration, e.g. see figure 2.5. This indicates that the clay doesn't affect the the flow pattern for low clay concentrations($\leq$1.5 wt.%). For these concentrations all of the clay ended up around the equator on the drop surface.

The reason the clay ends up on around the equator on the drop surface, can be described as a combination two things, the flow and that the clay particles reduce the the interfacial energy when on the interface between the drop and the surrounding fluid. The flow in combination with the fact that the clay is heavier(higher mass density), will cause the particles to be forced outwards towards the drop surface due to the centrifugal force from the flow inside the drop. Once at the drop surface the particles will get trapped there at the interface as described by Ramsden. The direction of the flow and the fact that the flow is zero at the equator and the poles, equation (2.22), will determine where the particles end up. In our case, silicone drop in castor oil, we have flow from the poles towards the equator($RS < 1$), so the clay ends up at the equator. Theoretically, we should be able to let the clay form at the poles by using a drop-fluid combination with $RS > 1$.

During the time the ring is created, it is also seen that clay particles coming in contact with each other, have a tendency to stick together. This is most

probably due to the polarization of the clay particles, so that opposite poles on the particles will attract each other when close enough, and then sticking together.

The results for ring size over time for 0.5 wt.%, 1 wt.% and 1.5 wt.% Na-Fh concentration were shown in figure 5.2. It is clear that higher clay concentration results in wider rings, which seems obvious. The fact that the ring grows in size faster for higher fields, is also expected according to theory, since the flow velocity and tangential stress increases with increasing fields. When it comes to final ring size, we see that there are large differences between rings made in 100 V/mm and 200 V/mm for the 1 wt.% and 1.5 wt.% drops, but almost no difference in the 0.5 wt.% drop. One explanation to the large difference for the 1 wt.% and 1.5 wt.% drops can be that not all of the clay had reached the drop surface yet. From the plot we can see that ring sizes are still growing towards the end of the measurements, so it's likely the rings could have gotten even bigger if measured over a longer period of time. This is also seen from the photos in figure 5.3, where clay particles still can be seen inside the drop after 3 min in a 100 V/mm field, so for the 100 V/mm case, the ring most likely would have gotten even larger.

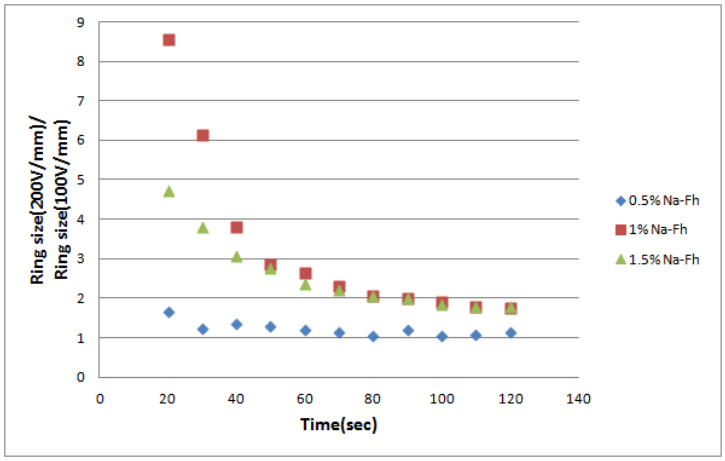

Figure 6.1: Plot showing the scale between ring sizes in 100 V/mm and 200 V/mm for different concentrations. Drop radius ∼0.775 mm.

The time however doesn't seem to be the only explanation. In figure 6.1 we can see the ring size scaling factor over time between 100 V/mm and 200 V/mm fields for each of the concentrations. As we can see the rings of drops with 1 wt.% and 1.5 wt.% clay in 200 V/mm field have almost twice the size of those in 100 V/mm field after 2 min. The few remaining particles inside drop doesn't seem enough to make up for the large difference between 100 V/mm and 200 V/mm. The electric field will align the clay particle dipoles along its field lines. The particles align along the field lines due to the torque arising on the dipole in the electric field, the same electric force causing this torque and alignment, will try to stretch the dipoles along the field. This results in the ring, formed by clay dipole chains, to stretch out towards each electrode and thus increase in size. The fact that the increased ring size in higher fields is mostly caused by the electric force, and not just because more particles has reached the surface, can also be seen from figure 5.3. If we look at the rings in 200 V/mm for 1 wt.% and 1.5 wt.% we can clearly see they appear thinner(lighter in color), than the ones in 100 V/mm, indicating they indeed are stretched out, and not just containing more clay particles. This was also confirmed by lowering and increasing the field, which resulted in narrower and wider ring, respectively. The large difference seen early in figure 6.1 between 100 V/mm and 200 V/mm, is because of the different flow velocities in the two fields as already discussed is in agreement with Taylors model. The fact that 1 wt.% has a larger difference than 1.5 wt.% could be a result of the higher clay concentration inside the drop initially in the 1.5% drop. The higher clay concentration should result in higher conductivity, which again would result in a larger RS and thus lower flow velocity according to eq. (2.22). As we can see, when some time has passed, and naturallly the clay concentration inside the drop lowers, the difference between 1 wt.% and 1.5 wt.% evens out. The reason for the 0.5 wt.% drops ring not to stretch out, is possibly due to less clay particles, thus less dipoles and charges, so less electric force is exerted on the ring.

The plot in figure 5.4 shows the ring size difference for individual drops from the same sample. The large difference is believed to arise from different clay concentration in each drop. Even though each drop is from the same sample, and the sample has been mixed well, concentration differences could be caused by sedimentation in the sample during the experiment. During our experiments the sample was only hand shaken for every fifth drop, if the sample had been kept on a magnetic stirrer during the experiments, not only before, we could perhaps have gotten more even drops.

Comparing the ring sizes for different clay types showed that Na-Fh, Laponite RD and Laponite S behaved similarly, while 3CEC-Fh bahaved different, figure

5.5. The larger ring size in Na-Fh than in the two Laponite samples is possibly caused by the concentration differences, from table 4.2, we can see that Na-Fh had an actual concentration of 1.11 wt.%, while Laponite RD and S had 0.93 wt.% and 0.99 wt.%, respectively. This seems to be in good agreement with whats observed in the plot. When it comes to 3CEC-Fh and its larger ring size, despite lower actual concentration than Na-Fh, it seems this could only be explained by that 3CEC-Fh forms chains easier as shown by Rozynek[22], and thus would be more affected by the electric forces stretching the ring.

Even though Na-Fh and Laponite had corresponding ring sizes when taking the actual concentrations into account, we did see a difference in ring shape. The rings made in the Laponite drops were more even in size around the equator, as shown in figure 5.6. Laponite was already a very fine powder when supplied from the manufacturer, finer than I was able to make the Na-Fh clay. This gave Laponite very even sized and small particles, which resulted in a more even clay particle distribution inside the drop, compared to Na-Fh where particle sizes can vary some and cause a more uneven particle distribution inside the drop. It is believed that this is what causes the more even ring for the Laponite drops too.

When it comes to the antiring experiment, i.e. reversing the flow, this experiment was unsuccessful. The biggest problem was the low viscosity of the silicone suspending fluid, which resulted in the drop moving to fast. When mixing 100cST and 10000cST silicone oil to make a more viscous suspending fluid, we only saw prolate deformation and break-up for low fields, $\sim$ 200 V/mm, which is about half of what we expected to need for flow velocities similar to the silicone drop case. The prolate deformation was expected, which is in agreement with theory for $RS > 1$. But since we didn't observe any flow, it would appear that the castor oil drop acted as a conductor, not a leaky dielectric. Even though making the antiring by reversing the EHD flow should be theoretically possible, no previous research has been found that shows this. The closest have to be the antiring made with the dielecrophoresis(DEP) effect by Hwang *et al.* in AC field. In DEP the particles behave similarly to what they would have in EHD for the same drop-fluid suspensions. Except its no flow in DEP for AC fields. It could be interesting to study this furder with other combinations of oils, to try and get the antiring in DC too. The EHD flows in DC affects a larger part of the surrounding fluid around the drop compared to DEP which only happens in regions with non-uniform field, which is close around the drop. In emulsions it could be important to affect large or small areas, so fully understanding the difference between DEP and EHD could be useful to better stabilize or destabilize emulsions.

6.2 Chains

We've already talked about the polarization of clay particles and how they attract eachother. We saw how the ring size could be increased by increasing the electric field due to stretching of the ring towards each electrode. By increasing the field enough, we are able to stretch the ring across the entire drop. When doing so, the drop got a prolate deformation instead of an oblate deformation. This could be due several things, one is that the electric forces acting on the clay particles are so strong, so when the clay covers the entire drop and has no more room to move, the drop gets stretched with the clay chains. This is ofcourse dependent on the clay being a surfactant. Being a surfactant would mean that some energy would be required to pull the surfactant of the drop-fluid interface, according to Ramsden. This will cause the drop to deform instead, until enough energy is applied to remove the particles from the interface. Another cause is that the clay chains form so strong bonds, that the EHD flow is limited, and thus reducing the the stress caused by the flow resulting in less oblate deformation. This is most likely for higher clay concentration drops though, as the chains would have to be inside the drops also. A third possibility is that the clay chains act as conductors when stretching across the drop, and thus changing the value of RS for the system. By raising RS enough, the drop would get a prolate deformation according equation 2.20. If the chains cause the entire drop to act as an conductor instead of a leaky dielectric, only prolate deformation can happen as well.

The way the field is applied also has consequences for the drops development. If we remember from figure 5.8 we see that the drop shape is very different if a high field is applied initially, or if a ring has been made in a low field first. If a high field is applied right away, we get a smooth oval drop shape, and the prolate deformation slowly reduces over time. As the drops prolate deformation decreases, more and more clay paricles end up on the drop surface. This could mean as the clay concentration inside the drop gets lower, the conductivity goes down, which again would explain the reducing prolate deformation. By creating a ring first however, we are able to get a constant prolate deformation for the same field strength as we had reducing deformation if no ring were made first. The drop shape is also more square. The square shape is most likely the strong bonds in the chains and the electric force stretching the chains along the field lines, preventing the surface tension to make the drop spherical. Since constant prolate deformation is possible for this case, it would seem that by making the ring first, the conductivity of the chains, or the electric force acting on the chains is somehow improved. This could be because better and more compact chains

are possible if all the clay are packed together in a tight ring first, compared to being spread evenly across the drop surface if the initial field is high.

6.3 AC

In our experimentts we saw alteranting flow and oscillating deformations up to 3 Hz. The direction of the flow was the same as the one seen in DC fields. This was expected according to theory since flow velocity and durection is dependent on E^2. Even if we saw flow up to 3 Hz, we only observed formation of a ring up to ~ 0.25 Hz, shown in figure 5.9. This is probably caused by the frequency getting to high compared to the Maxwell time $\frac{1}{\tau}$. Each time the field alternated(square signal), it took about ~ 1 second for the drop to reach maximum deformation and for the flow to reach maximum velocity. So its clear that compared to a DC field, the average flow velocity will get lower with increasing frequency. This is a good indicator that it really is the leaky dielectric flow which causes the the clay to end up on the surface and form the ring.

As the frequency got increased towards 0.25 Hz we also observed how more and more chains where created inside the drop. These chains are caused by the polarization of clay particles, and since there is little or no viscous flow, the chains wont get dragged apart, and are able to maintain their form. This could be useful in elecrorheological fluids. A fluid with polarizable particles and no drops, would create chains in both DC and AC fields, if we had an ER emulsion with drops containing the polarizable particles we could both build up chains in AC field, and tear them down in DC fields. The build up of chains will strengthen the material properties, while tearing the chains down will soften the material properties.

Trying to form chains in a cell filled with castor oil mixed with clay was done to see if the induced viscous flows in a DC field could tear up chains outside the drop also. We also wanted to compared this with a drop in AC field. The results showed us what we expected, that no flow was seen outside the drop in AC field, and thus the chains were only affected by the drop falling, and in DC field, the viscous flows broke up chains around the drop. The maximum voltage we could get for the AC amplifier as 3 kV, resulting in a 300 V/mm field for our cell. This resulted in a weak chains, so it could be interesting to look at higher fields in the future, by using a smaller cell or another ampilfier, to see if chains could be strong enough to hold drops stationary in AC fields. The results of this could also be interesting in the field of ER-fluids and emulsions, since in this case one could also change ER properties by changing between AC and DC

fields.

6.4 Modified clay

The modified clay displayed different behavior than non-modified. For the 0.5 wt.% and 1.5 wt.% 3CEC-Fh drops, we observed that chains were formed easier, and more affected by stretching from the electric force, figure 5.11. It has been shown that modified clay particles align easier in an electric field and has higher conductivity and dielectric constant, than non-modified clay[21, 22], this could then be the reason for the increased stretching caused by the electric field, since this would cause a larger total polarization.

The prolate deformation of the drop and the fact that Taylor characteristic flow stopped early for 1.5 wt.% 3CEC-Fh compared to 1.5 wt.% Na-Fh could be caused by a couple of things. The increased stretching of the chains, would cause the drop to stretch too, just like seen in higher fields for Na-Fh drops. Since the chains formed easier, they could possible hold together stronger too, and this would make them harder to brake up, which again would lead to better conductivity. So the fact that the viscous flow stopped early, could be a result of long chains forming during this time and thus changing the drop into a conductor, which would result in different flow velocities and prolate deformation. Another thing to remember is the actual clay concentrations, from table 4.2, we can see that the 1.5 wt.% 3CEC-Fh sample had a higher concentration compared to the 1.5 wt.% Na-Fh sample, which would result in a larger ring, and thus more chains could be made.

For the 1 wt.% 3CEC-Fh sample, we also saw a wider ring despite actual lower concentration compared to Na-Fh sample, and the ring was more like a hemisphere, forming around the drop pole facing the negative electrode. From the pictures in figure 5.10, it doesn't appear like there is as much stretching of the clay, as seen for the 0.5 wt.% and 1.5 wt.% samples. So the increased ring size should be caused by the fact that the modified clay is lipophilic and disperse easier in oil than non-modified clay , which can be seen clearly in figures 3.2 and 3.3. This will cause a more even concentration throughout the sample, and thus increase the chance that every drop contains the right concentration of clay. The reason for a hemisphere forming instead of a ring around the equator, is not yet fully understood. We know that the clay nano-plates have a net negative charge, due to the negative charges on the plate surface dominate over the positive charges on the plate edges. During CTAB modification, the CTAB adsorbtion happens with the negative charges the clay plate surface[22], leaving

a net positive charge from the positive charges at the clay plate edges. A net positive charge in the clay particles in our drop would explain the attraction against the negative electrode seen for the hemispheres in figure 5.10. However the clay plate charges should be neutralized by ions in the oil, if not we should have seen hemispheres forming against the positive electrodes for non-modified clay. So even if it seems the modified clay has some net positive charge, it is unclear what causes it.

What we do know, is that the forming of the clay hemisphere, naturally leaves one hemisphere clay free. As the clay hemisphere was formed, we could see increasing horizontal movement of the drop towards the positive electrode. The flow still looked like taylor flow, so the horizontal movement is most likely caused by the asymmetrical flow that arises since half of the drop is covered in clay. So the flow from the pole towards the equator on the drop side facing the positve electrode, will result in a net horizontal propulsion of the drop, unlike the axisymmetrical flow seen in non-modified clay drops, where the propulsion from the flows on each side of the equator cancel each other out. The hemispheres also has a resemblence to Janus particles. A Janus particle is a particle whose surface has two or more distinct types of properties[25]. This could result in interesting behavior in an emulsion, since it's likely the drops with hemispheres will interact differently than drops with rings.

6.5 Rotation

For high fields and low clay concentration drops($\leq$1.5 wt.%), rotation was seen. For the pure silicone drop rotation didn't occur until the field had reached $\sim$980 V/mm. The transition from leaky dielecric flow to rotation was sudden, as the drop got a large tilt angle and larger deformation. It appeared that the rotational axis was perpendicular to the electric field, but hard to say in some cases, since the rotational axis wasn't always in a plane perpendicular or parallel to the camera. Measuring the rate of the rotation would be highly uncertain without some kind of tracer particles, this is also the case for rotation of drops containing clay. In pure drops, there are no reference points showing the rotation, while in clay drops, its too hard to distinguish clay particles from each other, so keeping track of one particle over several videoframes would be nearly impossible. Lighting the drop up, e.g. with a lasersheet, and adding distinguishable tracer particles could be a good way to track the rate of the rotation. Measuring the tilt of the drop was also a bit uncertain due the reason it was hard to see which way the drop tilted.

For 1 wt.% and 1.5 wt.% drops, the behavior was very similar to quincke rotation. For the 0.5 wt.% drops, a more chaotic rotational flow was seen. In the 0.5 wt.% case, the rotation occured in vortices on the drop surface, instead of the entire drop rotating. It is unclear what causes this. Chaotic quncke rotation have been observed for high fields, where the rotation rate and rotation direction changes randomly[26], but the rotation for our drop in 0.5 wt.% seems to be different from this. Maybe the leaky dielectric flow pushing from each side of the equator causes some instability in the ring, and thus causing the chaotic behavior.

From the phase diagram in figure 5.12, we can see that the critical field for where rotation occurs, gets lower with increasing clay concentration. This is very interesting, since it is the opposite of what you would expect from theory. Higher concentration of clay, should increase the conductivity of the drop, and thus should increase the critical field needed to achieve rotation, and even prevent it if RS got bigger than 1, that is when the dipole moment align with the electric field, causing a stable equilibrium. It is however important to remember how the rotation started. In pure silicone the rotation started right away if the field was high enough. This was not the case for the clay drops, here Taylor flow started when the field was applied, then after some time($\sim$1 min, depending on field strength) when all clay had reached the drop surface, the drop eventually started rotating. So this could indicate that drop conductivity only is increased while clay is inside the drop, but not on the surface. The fact that higher clay concentration results in lower critical field to achieve rotation, could be a result of the clay containing more charges, and thus making the the drop dipole more unstable in the electric field, which again will require a lower electric field to displace the dipole orientation.

6.6 Deformation and Break-up

It has been clear from our results that clay has a large impact on the deformation of drops. The clay results in a time dependent deformation, unlike pure silicone drops where the deformation is almost instant and time independent.

In figure 5.17 we see the oblate deformation comparison between pure silicone drops and 0.5 wt.% Na-Fh drops. Here the deformation is very much alike. There are three points of interest. One is the very oblate deformation for pure silicone in 980 V/mm, this huge jump is caused when the drop starts to rotate. For 0.5 wt.% the deformation pretty much is the same as the pure drops until 550 V/mm, then the deformation is less oblate. From video analysis it was clear

that at this field strength, the ring was stretched, causing the shift towards prolate deformation. At 600 V/mm the 0.5 wt.% drop is more oblate again, this is while the drop is rotating, and thus there is no more stretching of chains along the field direction.

For the 1 wt.% and 1.5 wt.% drops, the time dependence started to be a factor. Not only did the deformation increase over time, it changed from prolate to oblate also. As we can see from the plot in figure 5.18 all drops who started out with prolate deformation, ended up oblate. The 1 wt.% drops had a higher initial deformation than the 1.5 wt.% drops, which was unexpected, since prolate deformation should increase with conductivity, and thus with clay concentration. If we look at figure 5.19 we can see the final deformation for each of the concentation types. It is clear that higher clay concentration increases the oblate deformation. At 600 V/mm the stretching of the clay chains causes the deformation to shift towards prolate again. This increase in deformation can be explained by two things. Firstly, the clay could change the electric properties of the drop, increasing RS. Secondly, we know the clay gathers on the drop surface after a while when Taylor flow occurs. The clay could act as a surfactant reducing the interfacial tension. Both of these things would result in a larger deformation according to eq. (2.21).

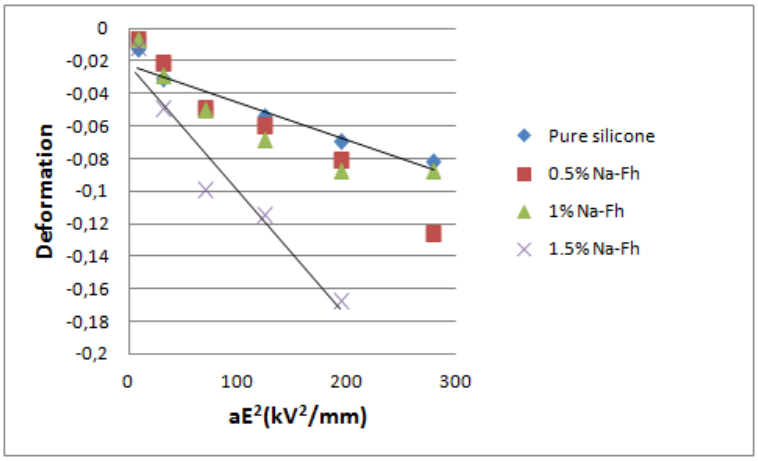

Figure 6.2: Plot showing deformation vs aE^2. Linear regression of D vs aE^2 for pure silicone drops($m \approx -2 \times 10^{-10}$ m/V^2) and 1.5 wt.% Na-Fh drops($m \approx -8 \times 10^{-10}$ m/V^2) shown. Initial drop radius ~0.775 mm.

In figure 6.2 we can see the linear regression m of deformation vs aE^2 for pure silicone drops and 1.5 wt.% Na-Fh. For pure silicone drops we have $m \approx -2 \times 10^{-10}$ m/V^2 and for 1.5 wt.% Na-Fh we have $m \approx -8 \times 10^{-10}$ m/V^2, while 0.5 wt.% and 1 wt.% are not shown, but clearly between pure silicone and 1.5 wt.%. The predicted slope m^* by eq. (2.21) would be $m^* \approx -9 \times 10^{-10}$ m/V^2 using the values from table 4.1, which is not that much larger than whats observed for 1.5 wt.% Na-Fh, which is 11% lower. Using the dielectric constant given by Vizika *et al.* gives an even larger difference with $m^* \approx -12 \times 10^{-10}$ m/V^2. The predicted m^* is for pure silicone oil however, and as we can see, the difference is much larger here, almost 80% lower than the predicted value. This large difference could be due to experimental errors, but was somewhat expected. Taylors model is only valid for small deformations since he derived his formula as an expansion/perturbation around a sphere. It has been observed that for large deformations(D < -0.02) the predicted deformation significantly diverge from experimental results[2, 24]. So for our case, when most of our measurments have been done in high field strengths resulting in large deformations, the difference between experimental results and predicted results should not be a surprise. This means however that the deformation seen in clay drops, shouldn't be compared to the leaky dielectric model in these high fields, but rather to the experimentally observed pure silicone drops.

The initial prolate deformation should be caused by increased conductivity from the clay particles. As the particles are transfered to the surface by the Taylor flow, the conductivity goes down, as well as the prolate deformation. The reason for the 1 wt.% drop to have larger initial prolate deformation isn't completely understood. It could be that the higher concentration of clay, causes more particles to bond in chains quicker. If we remember the chains could be stretched out by increasing the field strength, but they are also bonded together, so they could perhaps also prevent prolate deformation by their chain bonds holding the drop more together in the 1.5 wt.% drop. Another possibility is that the clay covers the drop surface faster in the higher clay concentration drop, and as just discussed, it was a possibility that the clay made the drop into a better dielectric when covering the surface. And if the surface gets covered quickly, this could be the reason the drop doesn't get such a large initial prolate deformation in the 1.5 wt.% drop.

For 2 wt.% and 2.5 wt.% drops the behavior was similar to what was observed for 1 wt.% and 1.5 wt.% drops, just more prolate tendencies, and initial prolate deformation happened for lower fields, as can be seen in figure 5.21. We just discussed how it's most likely the increased conductivity in the drops which causes the initial prolate deformation, and the Taylor flow carrying the clay to

the surface, which ensures the transition to more oblate deformation over time. The reason this transition last longer for drops with higher concentration of clay, should be caused by the fact that the deformation is happening at lower field strengths, when compared to lower clay concentration drops. Since the field strength is lower, the Taylor flow is slower, and thus it takes longer for the clay particles to travel to the surface.

At ∼3 wt.% there seems to be a transition from oblate final deformation, to just prolate deformation. The field regions from where nothing happened(no deformation) to break-up were short for drops with high clay concentrations(<100 V/mm), as can be seen in figure 5.12. From this figure it is also clear that deformation and break-up happens for lower field values as the concentration increases. But the behavior was almost exactly the like for 3 wt.%, 4 wt.% and 5 wt.% as can been seen in figure 5.22. Here we can see the transition between no deformation, to constant prolate deformation, to increasing prolate deformation for each clay concentration. The reason for no more oblate deformation in high clay concentration drops, should be caused by the high conductivity from all the clay, and thus giving a the drop a dipole aligned with the field so that only prolate deformation can happen, $RS > 1$.

Viscous flow stopped early too for high clay concentration, this seemed to be because chains formed throughout the drop, The formation of the chains could affect the flow in two ways, firstly the formation of chains could help increase the conductivity between the drop poles, making the drop into a conductor. Secondly the chains themselves could be so strong that they wouldn't break for the viscous flow, and thus causing drag on the flow. When chains had formed, a few particles also kept bouncing between the drop poles inside the drop. This could only be caused by the particles picking up electric charges and exchanging them between the poles.

When it comes to drop break-up this was seen for all concentrations, except pure silicone, 0.5 wt.% and 1.5 wt.% drops in field strengths below 650 V/mm. As seen in the result chapter, we observed two types of break-up happening from prolate deformation, and one type by oblate deformation. The reason for break-up is because the deformation get so large, that the interfacial tension no longer can hold the drop together. For low concentrations the break-up, see figure 5.24, happens as a combination of type (1) and type (2) break-up as described by Allan and Mason. That is a combination of conductive drop break-up, and break-up of a dielectric drop wit $RS > 1$. This is a clear indication of the clay increasing the conductivity of the drop. The bridging, see figure 5.23, seen for higher clay concentrations is probably a variation of the same type of break-up, but it would seem the clay particles have strengthened the drop, resulting in it

not breaking apart. This strengthening is most likely from the bonding chains made by the clay particles. This strengthening could be a useful aspect, because if allows for bigger prolate deformations without break-up, which can be useful if drop coalescence is of importance, for example in destabilizing emulsions, but also as a electrorheological fluid.

The collapsing drop seen in very high fields, figure 5.25, is similar to type (3) break-up described by Allan and Mason, which was for a dielectric drop with $RS < 1$. For so high fields only pure 0.5 wt.% and 1 wt.% Na-Fh drops were tested, and the collapsing was only seen for the 0.5 wt.% and 1 wt.% drops. This would indicate that the clay drops had lower RS compared to a pure silicone drop, since the silicone drop didn't collapse at this field strength. Meaning the conductivity has lowered and/or dielctric constant has been increased in the clay drops. This is very interesting, since in the results for break-up type (1) and (2) indicated that the drop conductivity increased with adding clay. The collapse at high fields, occured after rotation, and thus when most of or all clay was on the drop surface. So a possible explanation is that the conductivity and dielectric properties are not just dependent on clay concentration, but also how the clay is distributed in the drop. So it would seem RS increases when the clay is inside the drop, and lowers when on drop surface, just like we discussed for the initial prolate deformation at lower electric field strengths. The fact that the drop collapses, and ends up mixed with castor oil could be a useful way of stabilizing emulsions.

6.7 Errors

There are a few things that could have caused errors in these experiments. The actual process of taking a drop from the sample, to the cell was important to keep the same for each drop. Placing different drops in different places in the cell, could cause different fields, and thus affect the results. Also when taking the drops from the sample, it was important to take the drops from the same depth in the sample glass. Because of sedimentation in the sample, the clay concentration would increase towards the bottom of the glass. So by taking drop samples from different depths, drops could contain different clay concentrations. Reducing the possible error caused by sedimentation could be done by keeping the sample under continous mixing during the experiments also.

Another thing that would affect sample concentration, was different clay particle sizes in the different clay types. So clays containing large particles, would sediment faster, resulting in lower concentration towards the top of the

sample glass, from where the drops were taken from. This was hard to avoid, even when using a pestle and mortar the industrial made clay would contain finer and more even sized particles. The size of the particles could possibly also affect the behavior of the drop, e.g. the more even ring observed for Laponite clay, compared to Na-Fh clay.

The fact that modified clay disperse better in oil, and thus take up more volume compared to non-modified clay, will result in a difference when comparing volume concentrations. While we mixed samples by weight, a better way would probably be to mix samples by volume instead.

Making the samples should also be done under the same conditions, temperature, humidity etc. During our several experiments, samples where made along the way and the condititions weren't recorded, so no guarantee that the samples were made under the same conditions. This could result in more than just concentration difference between the samples. It is known that the clay can absorb water. A recent measurement by Zbigniew Rozynek at NTNU has shown that the conductivity in clay changes with air humidity. This could affect how our clay particles would act in a electric field. So to avoid clay samples with different conductivities they should be made at the same time, and ideally kept at high temperature to remove all water. A plot showing the results from Rozyneks conductivity measurements can be seen in figure B.4.

A difference in conductivity between the different clay-oil samples, could be a reason for not seeing initial prolate deformation and break-up in the 1.5 wt.% Na-Fh sample for electric fields strengths which caused this in the 1 wt.% Na-Fh sample. The same could be said for the 2.5 wt.% Na-Fh sample, for which we saw prolate deformation and break-up for lower field strengths than for the 3 wt.% and 4 wt.% Na-Fh samples.

6.8 Reversibility and drop control

In the result chapter we looked a bit at how changing the field would affect the drop, opposed to just letting a constant field be applied. Knowing if a process is reversible or not is of great importance if you want the abilty to control the process. We discovered that by changing field strengths, we could adjust ring size(by streching) and the deformation of drops.

Another discovery was that the initial prolate deformation seen in drops with 1-2.5 wt.%, was a one time occurrence. This means we can avoid, a large initial deformation or break-up by applying a low field first, let the clay settle on the drop surface , and then increase the field without having any prolate

deformation or break-up, which we would have had if the initial field had been high. The same goes for rotation. The drop could be made to rotate in lower fields than seen before by getting rotation in a high field, and then lowering the field.

6.9 Concluding remarks

In this study we have seen how adding clay particles to silicone oil drops suspended in castor oil drastically alters the drops behavior when in an electric field compared to pure silicone oil drops.

The results have shown that clay particles change the conductivity and dielectric properties of the silicone oil drops. Dependent on the drops clay concentration, larger oblate deformation and drop rotation can be achieved in electric field strengths different from that of a pure silicone oil drop, in addition prolate deformation and break-up have been observed for drops with clay, which haven't been observed for pure silicone oil drops. Results have also shown that the drop behavior becomes time dependent in an electric field when clay particles are added, unlike pure silicone oil drops which almost instantly achieves a steady state.

For low clay concentrations and electric field strengths, the leaky dielectric flow will cause the clay particles to gather on the drops surface forming a ring around the equator or cover the entire surface with increasing electric field strength and clay concentration. With increasing clay concentrations the drops behavior goes from that of a leaky dielectric drop with $RS < 1$, to that of a leaky dielectric drop with $RS > 1$, or even a conducting drop.

The different types of drop behavior resulting from adding clay particles could be useful in EHD systems, emulsions and ER fluids.

6.10 Future suggestions

More work is needed to to fully investigate the effects of clay particles in oil. Future work and experiments could focus on better sample preparations to remove the uncertainty in conductivity due to humidity, and also different particles could be useful. Particles with more even or the exact same sizes would be a huge improvement when it comes to the concentration uncertainty. A study of non-conducting and unpolarizable particles could help give an insight in how the drop behaviors seen in this study are dependent on the clay particles

conductivity and their polarity.

Synchotron studies would be useful in determining what happens inside the drop, and especially to see how clay chain build up happens. Seeing when and how clay particles align and chains are formed, could help explain the different drop behaviors in different electric field strengths and for different clay concentrations. Especially to see if the build up of chains, and thus possibly the conductivity of the drop, is related to the time dependent deformation.

Drop and particle rotation has also been observed to change the viscosity[26] and conductivty[13] of the surrounding fluid. So a further study on this could also be interesting.

Use of clay in emulsions should also have some scientific interest. We have already seen how clay affect single drops, so a continuation of this study could involve multiple drop systems, i.e. emulsions.

List of Figures

List of Tables

Appendix A

A.1 Solution to the Laplace equation for a dielectric sphere in a dielectric medium

A solution to the Laplace equation for a dielectric sphere follows. The derivation follows to some extent [10]. Eq. (2.3) can be written

$$\frac{\partial}{\partial r}\left(r^2\frac{\partial V}{dr}\right)+\frac{1}{\sin\theta}\frac{\partial}{\partial\theta}\left(\sin\theta\frac{\partial V}{\partial\theta}\right)=0. \tag{A.1}$$

By separating the variables we can express the potential as a product of two functions:

$$V(r,\theta)=R(r)\Theta(\theta) \tag{A.2}$$

Combining eq. (A.1) and (A.2) and then dividing by $V(r,\theta)$ we end up with

$$\frac{1}{R}\frac{d}{dr}\left(r^2\frac{dR}{dr}\right)+\frac{1}{\Theta\sin\theta}\frac{d}{d\theta}\left(\sin\theta\frac{d\Theta}{d\theta}\right)=0. \tag{A.3}$$

We now have an equation which equals zero with two terms depending on two diffferent variables,r and θ, we can therefore conclude that each term is a constant, and we can seperate each term into two equations. The first term can be written

$$\frac{1}{R}\frac{d}{dr}\left(r^2\frac{dR}{dr}\right)=l(l+1) \tag{A.4}$$

which has a solution

$$R(r)=Ar^l+\frac{B}{r^{l+1}} \tag{A.5}$$

where A and B are any constant. The second term can be written

$$\frac{1}{\Theta \sin\theta}\frac{d}{d\theta}\left(\sin\theta\frac{d\Theta}{d\theta}\right) = -l(l+1) \tag{A.6}$$

which has one solution equal to the l'th Legendre polynomial in $\cos\theta$, which is:

$$\Theta(\theta) = CP_l(\cos\theta) \tag{A.7}$$

where C is any constant. The other solution to eq. (A.6) will blow up for each value of l around $\theta = 0$ and $\theta = \pi$, these components of the solution must be set to zero when the z-axis is accessible[10]. Combining the two solutions and merging the constant C with A and B we get the general seperable solution to the Laplace equation as

$$V(r,\theta) = \left(Ar^l + \frac{B}{r^{l+1}}\right)P_l(\cos\theta). \tag{A.8}$$

The general solution is then a linear combination of the different seperable solutions, which gives us

$$V(r,\theta) = \sum_{l=0}^{\infty}\left(A_l r^l + \frac{B_l}{r^{l+1}}\right)P_l(\cos\theta). \tag{A.9}$$

The sum over seperable solutions that do not diverge inside the sphere is

$$V_{in}(r,\theta) = \sum_{l=0}^{\infty} A_l r^l P_l(\cos\theta), \tag{A.10}$$

and outside the sphere we have a uniform field, boundary condition (2.6), in addition to the seperable solutions that converge to zero at infinity, which gives us

$$V_{out}(r,\theta) = -E_0 r\cos\theta + \sum_{l=0}^{\infty}\frac{B_l}{r^{l+1}}P_l(\cos\theta). \tag{A.11}$$

To fulfill a continous potential, eq. (2.4), we must require:

$$A_l a^l = \frac{B_l}{a^{l+1}}, \quad for\ l \neq 1 \tag{A.12}$$

$$A_1 a = -E_0 a + \frac{B_1}{a^2}, \quad for\ l \neq 1 \tag{A.13}$$

To fulfill the boundary condition for the perpendicular field at the sphere surface, eq. (2.5),we must require:

$$\epsilon_{in} l A_l a^{l-1} = -\epsilon_{out} \frac{(l+1)B_l}{a^{l+2}}, \quad for\ l \neq 1 \tag{A.14}$$

$$\epsilon_{in} A_1 = -\epsilon_{out} \left(E_0 + \frac{2B_1}{a^3} \right) \tag{A.15}$$

This gives us the following constants:

$$A_l = B_l = 0, \quad for\ l \neq 1 \tag{A.16}$$

$$A_1 = -\frac{3}{\epsilon_{in}/\epsilon_{out} + 2} E_0 \tag{A.17}$$

$$B_1 = \frac{\epsilon_{in} - \epsilon_{out}}{\epsilon_{in} + 2\epsilon_{out}} a^3 E_0 \tag{A.18}$$

Which gives us the final potential inside the sphere:

$$V_{in}(r, \theta) = -\frac{3E_0 r \cos\theta}{\epsilon_{in}/\epsilon_{out} + 2}. \tag{A.19}$$

and outside the sphere:

$$V_{out}(r, \theta) = -E_0 r \cos\theta + \frac{\epsilon_{in}/\epsilon_{out} - 1}{\epsilon_{in}/\epsilon_{out} + 2} \frac{a^3 E_0 \cos\theta}{r^2} \tag{A.20}$$

Where the second term in eq. (A.20) is the potential from the induced dipole.

Appendix B

Data

B.1 Figures

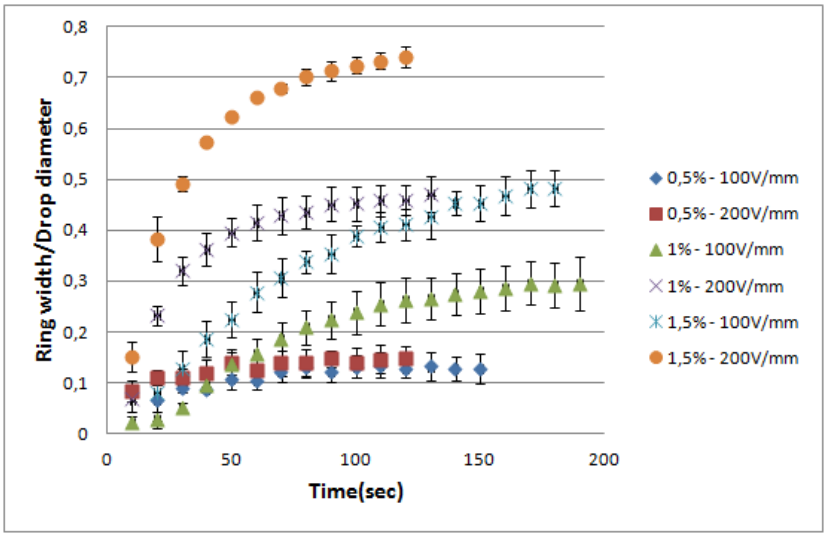

Figure B.1: Plot with standard deviation showing ring size over time for drops with 0.5 wt.%, 1 wt.% and 1.5 wt.% concentrations of Na-Fh in 100 V/mm and 200 V/mm fields. Drop radius ~0.775 mm.

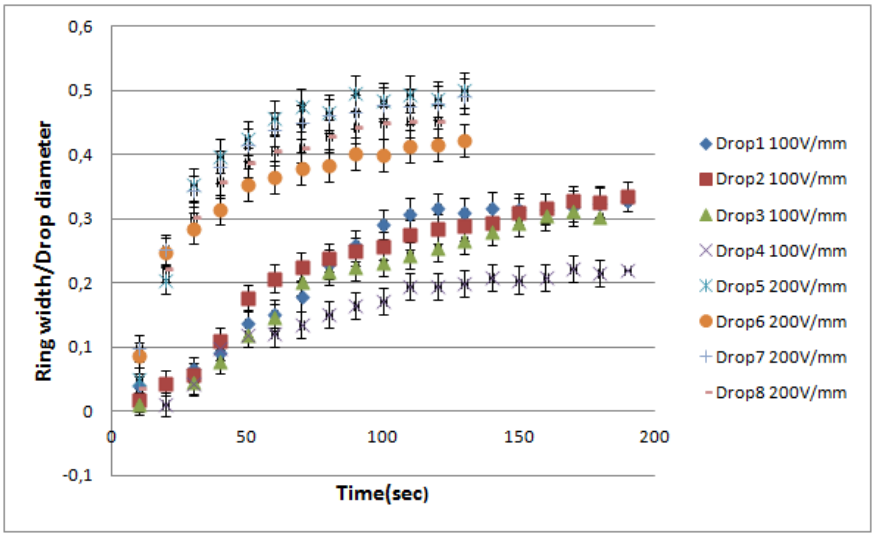

Figure B.2: Plot with errorbars showing ring size over time for individual drops with 1 wt.% concentrations of Na-Fh in 100 V/mm and 200 V/mm fields. Drop radius ∼0.775 mm.

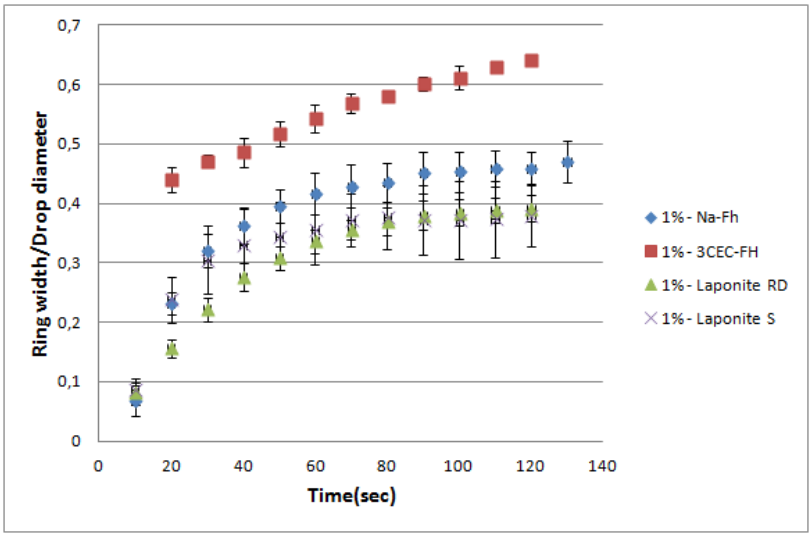

Figure B.3: Plot with standard deviation showing ring size over time for drops with different types of clay in a 200 V/mm field. Drop radius ∼0.775 mm.

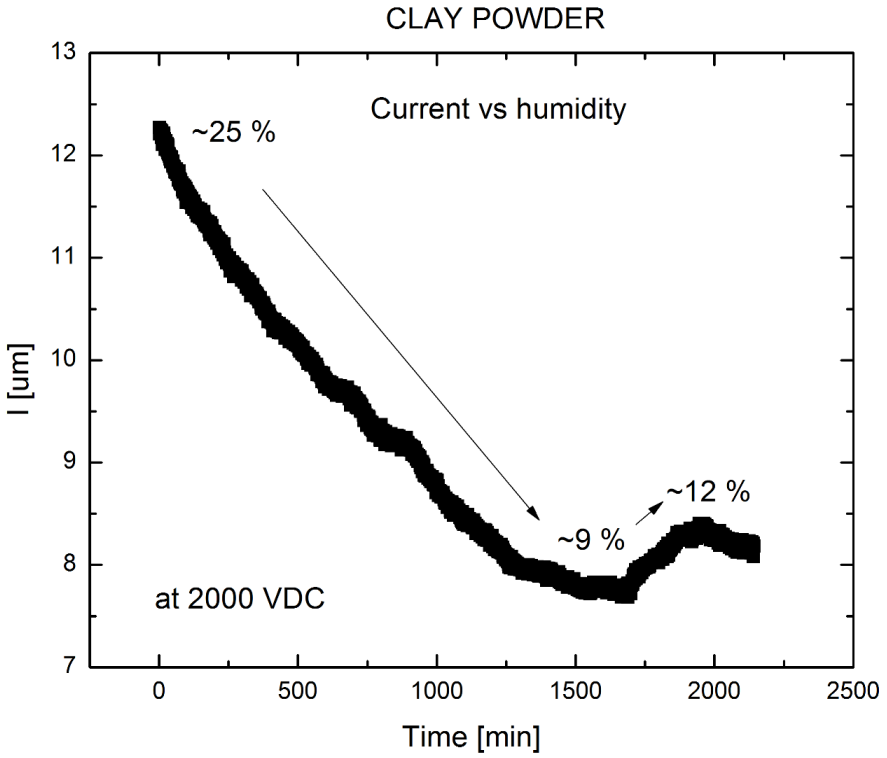

Figure B.4: Plot showing how conductivity of clay changes with humidity. Plot and measurements done by Zbigniew Rozynek at NTNU.

B.2 Videos

B.2.1 Video information

Here some links to some of the recordings done during this study can be found. Videos are intended as additional information for anyone who is interested. The url adresses are quite long, so if your reading the printed version of this thesis and want to see the videos, its recomended you get the pdf version first which includes hyperlinks. The pdf can be downloaded from

http://dl.dropbox.com/u/50702216/ClayOil.pdf.

In order to view the videoclips, you may need VLC, Media Player Classic or something similar.

All videos are filmed perpendicular to the electric field except one, which shows the ring formation at an angle with respect to the electric field. In the videos, the electric field goes from right to left. The connection betweeen the microscope and the camera inverted the image, so in the videos up is down and left is right. This results in the drop 'falling' upwards. Some focus issues, and movement of the cell to keep the drop in picture can occur. All drops have $\sim$0.775 mm radius. The videos are in no particular order with respect to this thesis.

B.2.2 Video links and description

Video1 - Shows a 0.5 wt.% 3CEC-Fh drop in a 100 V/mm electric field. A few chains form on the surface of the drop instead of a ring.

http://dl.dropbox.com/u/50702216/3CEC-FH0.5100Vmm.MTS

Video2 - Shows a 1 wt.% 3CEC-Fh drop in a 200 V/mm electric field. The clay particles form as a hemisphere on the drop pole facing the negative electrode(ground). As the hemisphere forms, the drop gradually starts to move towards the positive electrode.

http://dl.dropbox.com/u/50702216/3CEC-FH1200Vmm.MTS

Video3 - Shows a 1.5 wt.% 3CEC-Fh drop in a 200 V/mm electric field. Increasing prolate deformation with clay particle chains clearly visible.

http://dl.dropbox.com/u/50702216/3CEC-FH1.5200Vmm.MTS

Video4 - Shows a 1 wt.% Laponite RD drop in a 200 V/mm electric field. Filmed at an angle with respect to the electric field. Also show the more even ring Laponite forms compared to Na-Fh.

http://dl.dropbox.com/u/50702216/LapRD1200Vmm.MTS

Video5 - Shows a 0.5 wt.% Na-Fh drop in an increasing electric field. Calling out kilo voltage in video(in norwegian). Voltage ranging from 0-10 kV. Electrode seperation is 1cm. Drop collapsing seen in the higher fields.
http://dl.dropbox.com/u/50702216/Na-Fh0.50-1000Vmm.MTS

Video6 - Shows a 0.5 wt.% Na-Fh drop with an electric field starting at 400 V/mm and is adjusted up to 600 V/mm during the video. Chaotic 'snake'-like rotation occurs at 600 V/mm. Eventually the drop collides with another drop stuck at electrode, rotation still continues.
http://dl.dropbox.com/u/50702216/Na-Fh0.5400-500-600Vmm.MTS

Video7 - Shows a 1 wt.% Na-Fh drop in an elecric field starting at 200 V/mm, is then adjusted up to 500 V/mm, and then down to 200 V/mm again. Shows ring formation and how ring gets stretched in higher fields.
http://dl.dropbox.com/u/50702216/Na-Fh1200-500-200Vmm.MTS

Video8 - Shows a 1 wt.% Na-Fh drop in a 590 V/mm electric field. Large prolate deformation which reduces over time, the drop eventually ends up rotating.
http://dl.dropbox.com/u/50702216/Na-Fh1590Vmm.MTS

Video9 - Shows a 1 wt.% Na-Fh drop in a 640 V/mm electric field. The drop breaks up into two parts. One part hit electrode wall, the other part starts to rotate.
http://dl.dropbox.com/u/50702216/Na-Fh1640Vmm.MTS

Video10 - Shows a 3 wt.% Na-Fh drop in a 430 V/mm electric field. Increasing prolate deformation.
http://dl.dropbox.com/u/50702216/Na-Fh3430Vmm.MTS

Video11 - Shows a 4 wt.% Na-Fh drop in a 400 V/mm electric field. Slow bridge.
http://dl.dropbox.com/u/50702216/Na-Fh4400Vmm.MTS

Video12 - Shows a 4 wt.% Na-Fh drop in a 500 V/mm electric field(1). Fast bridge.
http://dl.dropbox.com/u/50702216/Na-Fh4500Vmm1.MTS

Video13 - Shows a 4 wt.% Na-Fh drop in a 500 V/mm electric field(2). Same drop as in video12, but after field has been applied $\sim$3 min. Video starts just before bridge starts to break up.

http://dl.dropbox.com/u/50702216/Na-Fh4500Vmm2.MTS

Video14 - Shows a pure silicone oil drop in a 1100 V/mm electric field. Shows how tilt suddenly increases when quincke rotation starts.
http://dl.dropbox.com/u/50702216/Puresiliconedrop1100Vmm.MTS

Bibliography

[1] J. R. Melcher and G. I. Taylor, "Electrohydrodynamics: A review of the role of interfacial shear stresses," *Annual Review of Fluid Mechanics*, vol. 1, no. 1, pp. 111–146, 1969.

[2] P. F. Salipante and P. M. Vlahovska, "Electrohydrodynamics of drops in strong uniform dc electric fields," *Physics of Fluids*, vol. 22, no. 112110, 2010.

[3] K. Hwang, P. Singh, and N. Aubry, "Destabilization of pickering emulsions using external electric fields," *Electrophoresis*, vol. 31, pp. 850–859, 2010.

[4] A. J. Simmonds, "Electro-rheological valves in a hydraulic circuit," *IEEE Proceedings-D*, vol. 138, pp. 400–404, 1991.

[5] M. Seed, G. S. Hobson, R. C. Tozer, and A. J. Simmonds, "Voltage-controlled electrorheological brake," *Proc. IASTED Int. Symp. Measurement, Sig. Proc. and Control*, 1986.

[6] R. Stanway, J. L. Sproston, and A. K. El-Wahed, "Applications of electro-rheological fluids in vibration control: a survey," *Smart Materials and Structures*, vol. 5, pp. 464–482, 1996.

[7] C. T. O'Konski and H. C. Thacher, "The distortion of aerosol droplets by an electric field," *The Journal of Physical Chemistry*, vol. 57, no. 9, pp. 955–958, 1953.

[8] G. Taylor, "Studies in electrohydrodynamics. i. the circulation produced in a drop by electrical field," *Proceedings of the Royal Society of London. Series A. Mathematical and Physical Sciences*, vol. 291, no. 1425, pp. 159–166, 1966.

[9] G. Quincke, "Ueber rotationen im constanten electrischen felde," *Annalen der Physik*, vol. 295, no. 11, pp. 417–486, 1896.

[10] D. J. Griffiths, *Introduction to Electrodynamics, 3rd edition.* Prentice Hall, 1998.

[11] R. Allan and S. Mason, "Particle behaviour in shear and electric fields. i. deformation and burst of fluid drops," *Proceedings of the Royal Society of London. Series A*, vol. 267, no. 1328, pp. 45–61, 1962.

[12] S. Torza, R. G. Cox, and S. G. Mason, "Electrohydrodynamic deformation and burst of liquid drops," *Philosophical Transactions of the Royal Society of London. Series A, Mathematical and Physical Sciences*, vol. 269, no. 1198, pp. 295–319, 1971.

[13] N. Pannacci, L. Lobry, and E. Lemaire, "How insulating particles increase the conductivity of a suspension," *Phys. Rev. Lett.*, vol. 99, p. 094503, Aug 2007.

[14] H. Sato, N. Kaji, T. Mochizuki, and Y. H. Mori, "Behavior of oblately deformed droplets in an immiscible dielectric liquid under a steady and uniform electric field," *Physics of Fluids*, vol. 18, no. 127101, 2006.

[15] S. Krause and P. Chandratreya, "Electrorotation of deformable fluid droplets," *Journal of Colloid and Interface Science*, vol. 206, pp. 10–18, 1998.

[16] J. Q. Feng, "A 2d electrohydrodynamic model for electrorotation of fluid drops," *Journal of Colloid and Interface Science*, vol. 246, pp. 112–121, 2002.

[17] W. Ramsden, "Separation of solids in the surface-layers of solutions and 'suspensions'," *Proceedings of the Royal Society of London*, vol. 72, pp. 156–164, 1903.

[18] S. U. Pickering, "Cxcvi.—emulsions," *Journal of the Chemical Society*, vol. 91, pp. 2001–2021, 1907.

[19] H. A. Pohl, "The motion and precipitation of suspensoids in divergent electric fields," *Journal of Applied Physics*, vol. 22, pp. 869–871, 1951.

[20] J. O. Fossum, "Physical phenomena in clays," *Physica A: Statistical Mechanics and its Applications*, vol. 270, no. 1-2, pp. 270 – 277, 1999.

[21] B. Wang, M. Zhou, Z. Rozynek, and J. O. Fossum, "Electrorheological properties of organically modified nanolayered laponite: influence of intercalation, adsorption and wettability," *Journal of Materials Chemistry*, vol. 19, pp. 1816–1828, 2009.

[22] Z. Rozynek, B. Wang, J. O. Fossum, and K. D. Knudsen, "Dipolar structuring of organically modified fluorohectorite clay particles," *The European Physical Journal E*, vol. 35, p. 9, 2012.

[23] J. O. Fossum, Y. Méheust, K. P. S. Parmar, K. D. Knudsen, K. J. Måløy, and D. M. Fonseca, "Intercalation-enhanced electric polarization and chain formation of nano-layered particles," *EPL (Europhysics Letters)*, vol. 74, no. 3, p. 438, 2006.

[24] O. Vizika and D. A. Saville, "The electrohydrodynamic deformation of drops suspended in liquids in steady and oscillatory electric fields," *Journal of Fluid Mechanics*, vol. 239, pp. 1–21, 1992.

[25] F. Li, D. P. Josephson, and A. Stein, "Colloidal assembly: The road from particles to colloidal molecules and crystals," *Angewandte Chemie International Edition*, vol. 50, pp. 360–388, 2011.

[26] E. Lemaire and L. Lobry, "Chaotic behavior inelectro-rotation," *Physika A*, vol. 314, pp. 663–671, 2002.